



HAL
open science

Stabilization of explicit coupling in fluid-structure interaction involving fluid incompressibility

Erik Burman, Miguel Angel Fernández

► **To cite this version:**

Erik Burman, Miguel Angel Fernández. Stabilization of explicit coupling in fluid-structure interaction involving fluid incompressibility. [Research Report] 2008. inria-00247409v1

HAL Id: inria-00247409

<https://inria.hal.science/inria-00247409v1>

Submitted on 7 Feb 2008 (v1), last revised 23 Oct 2008 (v4)

HAL is a multi-disciplinary open access archive for the deposit and dissemination of scientific research documents, whether they are published or not. The documents may come from teaching and research institutions in France or abroad, or from public or private research centers.

L'archive ouverte pluridisciplinaire **HAL**, est destinée au dépôt et à la diffusion de documents scientifiques de niveau recherche, publiés ou non, émanant des établissements d'enseignement et de recherche français ou étrangers, des laboratoires publics ou privés.



INSTITUT NATIONAL DE RECHERCHE EN INFORMATIQUE ET EN AUTOMATIQUE

Stabilization of explicit coupling in fluid-structure interaction involving fluid incompressibility

Erik Burman — Miguel A. Fernández

N° ????

February 2008

Thème BIO



*R*apport
de recherche



Stabilization of explicit coupling in fluid-structure interaction involving fluid incompressibility

Erik Burman*, Miguel A. Fernández†

Thème BIO — Systèmes biologiques
Projet REO

Rapport de recherche n° ???? — February 2008 — 37 pages

Abstract: In this work we propose a stabilized explicit coupling scheme for fluid-structure interaction problems involving a viscous incompressible fluid. The coupled discrete formulation is based on Nitsche's method with a time penalty term giving L^2 -control on the fluid force variations at the interface. The scheme is stable, in the energy norm, irrespectively of the fluid-structure density ratio. Numerical experiments, in two and three dimensions, show that optimal time accuracy can be obtained by performing a few defect-correction iterations.

Key-words: Fluid-structure interaction, Nitsche's method, fluid incompressibility, time discretization, explicit coupling, loosely coupled schemes, defect-correction method

Preprint submitted to Computer Methods in Applied Mechanics and Engineering.

* University of Sussex, UK; e-mail: E.N.Burman@sussex.ac.uk

† INRIA, REO team; e-mail: Miguel.Fernandez@inria.fr

Unité de recherche INRIA Rocquencourt
Domaine de Voluceau, Rocquencourt, BP 105, 78153 Le Chesnay Cedex (France)
Téléphone : +33 1 39 63 55 11 — Télécopie : +33 1 39 63 53 30

Couplage explicite stabilisé en interaction fluide-structure avec fluide incompressible

Résumé : Dans ce travail on propose un schéma de couplage explicite pour la résolution numérique de problèmes d'interaction fluide-structure comportant un fluide visqueux incompressible. La formulation discrète couplée est basée dans la méthode de Nitsche et le rajout d'un terme de pénalisation donnant un contrôle L^2 de la variation des contraintes du fluide sur l'interface. Le schéma est stable, dans la norme de l'énergie, indépendamment du rapport de densités fluide-structure. Des expériences numériques, en deux et trois dimensions, montrent qu'on peut obtenir une précision optimale en temps après quelques itérations d'un algorithme de Résidus Corrigés.

Mots-clés : Interaction fluide-structure, méthode de Nitsche, fluide incompressible, discrétisation en temps, couplage explicite, algorithme de Résidus Corrigés

1 Introduction

Computational Fluid-Structure Dynamics (CFSD) is of great importance in practically all engineering fields, from aeroelasticity to bio-mechanics problems (see, for instance, [29, 10, 12, 25, 31, 28, 33, 18, 15, 38, 2] and the references therein).

In this paper we address the numerical simulation of fluid-structure interaction problems involving a viscous incompressible fluid. This problem is particularly difficult to treat efficiently when the fluid added-mass, acting on the structure, is strong. In other words, when the fluid and solid densities are close. Indeed, in such situations, *explicit* coupling schemes, *i.e.* that only involve the solution of the fluid and the structure once (or just a few times) per time step (see [32, 34, 12] for instance), are known to give rise to numerical instabilities (see [25, 31, 7]).

Up to now, these instabilities have been overcome mainly through the use of *implicit* coupling schemes (see [27, 18, 14, 15, 8, 1]). Such an approach leads to a fully coupled problem at each time step, the solution of which often requires a high computational effort. Recent advances suggest the use of *semi-implicit* coupling schemes [13] (see also [35]), which involve a simplified fully coupled problem.

Although significant improvements have been achieved in the last years, to the authors knowledge, none of the existing strategies are able to allow fully explicit coupling without compromising stability. Theoretical explanations of this issue have been reported in [7, 17]. In particular, in [17], it is argued that no explicit scheme can be constructed which would be unconditionally stable with respect to the fluid-structure density ratio.

In this paper we propose a stabilized explicit coupling scheme, whose stability properties are independent of the fluid-structure density ratio. For the coupling of the fluid and the solid we use a formulation due to Nitsche, to which we add a stabilizing term giving L^2 -control on the fluid force variations at the interface.

Nitsche's method [30] (see [19] for a review) is a classical method for imposing essential boundary conditions weakly. Unlike the penalty method, it is consistent with the original differential equation. Indeed, optimal convergence is retained without perturbing the conditioning of the matrix. Recently, the Nitsche's method was proposed in a domain decomposition framework in [3]. It has then been extended to different multi-physics problems. Let us cite the coupling of the Stokes-Darcy problem [5], the coupling of elliptic-hyperbolic problems or problems with discontinuous diffusivities [6] with special focus on iterative solving. In the context of fluid-structure interaction, using implicit coupling, some results are given for vibration problems (acoustics) in [20] and for transient fluid-structure interaction problems with moving fluid domains in [21].

An explicit decoupling of the fluid and the structure using Nitsche's matching conditions alone is not stable. The key to stability is the penalty term on the fluid force fluctuations acting on the interface.

The main disadvantage of the method is that the weak consistency of the stabilization term is of order $O(\delta t^{\frac{1}{2}})$ only leading to a scheme that is too dissipative in practice. In order to enhance accuracy, we propose an improved explicit coupling scheme involving a few defect-correction iterations (see *e.g.* [37]).

The remainder of the paper is organized as follows. In the next section we introduce the fluid-structure interaction problem under consideration. The corresponding Nitsche's space semi-discretized formulation is described in section §3. Section §4 is devoted to the time-discretization. In particular, in paragraphs §4.1 and §4.2, we introduce the classical coupling schemes, implicit and explicit, and analyze their stability properties within the Nitsche's framework. Motivated by these results, in section §5, we introduce our stabilized explicit coupling scheme. We analyze its stability properties and provide a formal consistency analysis that highlights the optimality loss due to the stabilizing term. We then propose to recover optimal time-accuracy by performing a few defect-correction iterations. Numerical experiments illustrating the theoretical results, and the efficiency of the proposed scheme, are reported in section §6. Finally, a summary of the results and some conclusions are provided in section §7. Some of the results of this paper have been presented, without proof, in [4] as a brief note.

2 The coupled problem

We consider a low Reynolds regime and assume that the interface undergoes infinitesimal displacements. The fluid is described by the Stokes equations in a

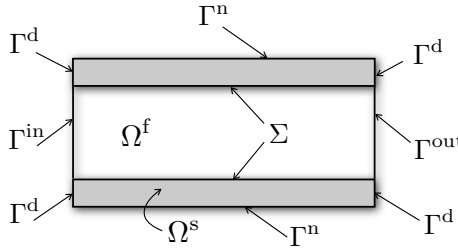


Figure 1: Geometrical description

fixed domain $\Omega^f \subset \mathbb{R}^d$, $d = 2, 3$. The structure is described by the classical linear elasticity equations in the solid domain $\Omega^s \subset \mathbb{R}^d$. We denote by $\Sigma \stackrel{\text{def}}{=} \partial\Omega^s \cap \partial\Omega^f$ the fluid-structure interface and $\partial\Omega^f = \Gamma^{\text{in}} \cup \Gamma^{\text{out}} \cup \Sigma$, $\partial\Omega^s = \Gamma^{\text{d}} \cup \Gamma^{\text{n}} \cup \Sigma$, are given partitions of the fluid and solid boundaries, respectively (see Figure 1). The coupled problem reads as follows: Find the fluid velocity and pressure (\mathbf{u}, p) and the structure displacement $\boldsymbol{\eta}$ such that

$$\left\{ \begin{array}{ll} \rho^f \partial_t \mathbf{u} - \nabla \cdot \boldsymbol{\sigma}(\mathbf{u}, p) = \mathbf{0}, & \text{in } \Omega^f, \\ \nabla \cdot \mathbf{u} = 0, & \text{in } \Omega^f, \\ \mathbf{u} = \bar{\mathbf{u}}, & \text{on } \Gamma^{\text{in}}, \\ \boldsymbol{\sigma}(\mathbf{u}, p) \mathbf{n} = \mathbf{g}, & \text{on } \Gamma^{\text{out}}, \end{array} \right. \quad (1)$$

$$\left\{ \begin{array}{ll} \rho^s \partial_{tt}^2 \boldsymbol{\eta} - \nabla \cdot \boldsymbol{\sigma}^s(\boldsymbol{\eta}) = \mathbf{0}, & \text{in } \Omega^s, \\ \boldsymbol{\eta} = \mathbf{0}, & \text{on } \Gamma^{\text{d}}, \\ \boldsymbol{\sigma}^s(\boldsymbol{\eta}) \mathbf{n}^s = \mathbf{0}, & \text{on } \Gamma^{\text{n}}, \end{array} \right. \quad (2)$$

satisfying the interface coupling conditions

$$\begin{cases} \mathbf{u} = \partial_t \boldsymbol{\eta}, & \text{on } \Sigma, \\ \boldsymbol{\sigma}^s(\boldsymbol{\eta}) \cdot \mathbf{n}^s = -\boldsymbol{\sigma}(\mathbf{u}, p) \cdot \mathbf{n}, & \text{on } \Sigma, \end{cases} \quad (3)$$

and the initial conditions $\mathbf{u}(0) = \mathbf{u}_0$, $\boldsymbol{\eta}(0) = \boldsymbol{\eta}_0$ and $\partial_t \boldsymbol{\eta}(0) = \mathbf{v}_0$. Here, ρ^f and ρ^s stand for the fluid and solid densities, $\boldsymbol{\sigma}(\mathbf{u}, p) \stackrel{\text{def}}{=} -p\mathbf{I} + 2\mu\boldsymbol{\epsilon}(\mathbf{u})$ and $\boldsymbol{\sigma}^s(\boldsymbol{\eta})$ for the fluid and solid stress tensors, μ for the fluid dynamic viscosity, $\boldsymbol{\epsilon}(\mathbf{u}) \stackrel{\text{def}}{=} \frac{1}{2}(\nabla \mathbf{u} + \nabla \mathbf{u}^T)$ for the fluid strain rate tensor, $\bar{\mathbf{u}}$ for a given velocity profile and \mathbf{g} for a given surface load.

Although (1)-(3) is a simplified linear coupled model, it features some of the main stability issues that appear in complex non-linear fluid-structure interaction problems involving a viscous incompressible fluid (see *e.g.* [25, 31, 7, 13]).

3 Nitsche's formulation: space semi-discretization

In this section, we provide a space semi-discretized formulation of the coupled problem (1)-(3). The fluid and structure equations (1)-(2) are discretized using, in both domains, standard finite elements techniques. The coupling conditions (3), on the contrary, are treated in a less standard fashion: by using Nitsche's penalty method.

In what follows, we will consider the usual Sobolev spaces $W^{m,q}(\Omega)$, with norm $\|\cdot\|_{m,q,\Omega}$, $m \geq 0$ and $q \geq 1$. In particular, we have $L^q(\Omega) = W^{0,q}(\Omega)$. We use the standard notation $H^m(\Omega) \stackrel{\text{def}}{=} W^{m,2}(\Omega)$. The norm of $H^m(\Omega)$ is denoted by $\|\cdot\|_{m,\Omega}$, in particular $\|\cdot\|_{0,\Omega}$ stands for the norm of $L^2(\Omega)$. Moreover, for each $X \subset \partial\Omega$, with $\text{meas}(X) > 0$, we define $H_X^1(\Omega)$ as the space of functions $v \in H^1(\Omega)$ such that $v|_X = 0$ in the sense of traces.

For the discretization in space, we introduce a family $\{\mathcal{T}_h^f\}_{h>0}$ ($\{\mathcal{T}_h^s\}_{h>0}$) of regular finite element triangulations of the domain Ω^f (resp. Ω^s). The subscript h refers to the level of refinement of the triangulations. Accordingly, let $W_h \times Q_h$ denote a conforming, inf-sup stable, finite element approximation of $[H^1(\Omega^f)]^d \times L^2(\Omega^f)$, and X_h a conforming finite element approximation of $[H_{\Gamma^{\text{in}}}^1(\Omega^s)]^d$. We also introduce the space $V_h \stackrel{\text{def}}{=} W_h \cap [H_{\Gamma^{\text{in}}}^1(\Omega^f)]^d$.

We may write the space semi-discretized Nitsche's formulation of (1)-(3) as: For all $t > 0$, find $(\mathbf{u}_h, p_h, \boldsymbol{\eta}_h, \dot{\boldsymbol{\eta}}_h) \in W_h \times Q_h \times X_h \times X_h$, with $\mathbf{u}_h = \bar{\mathbf{u}}_h$ on Γ^{in} , such that

$$\begin{aligned} & A^f((\mathbf{u}_h, p_h), (\mathbf{v}_h, q_h)) + A^s((\boldsymbol{\eta}_h, \dot{\boldsymbol{\eta}}_h), (\mathbf{w}_h, \dot{\mathbf{w}}_h)) \\ & - \int_{\Sigma} \boldsymbol{\sigma}(\mathbf{u}_h, p_h) \mathbf{n} \cdot (\mathbf{v}_h - \mathbf{w}_h) - \int_{\Sigma} (\mathbf{u}_h - \partial_t \boldsymbol{\eta}_h) \cdot \boldsymbol{\sigma}(\alpha \mathbf{v}_h, -q_h) \mathbf{n} \\ & + \gamma \frac{\mu}{h} \int_{\Sigma} (\mathbf{u}_h - \partial_t \boldsymbol{\eta}_h) \cdot (\mathbf{v}_h - \mathbf{w}_h) = \int_{\Gamma^{\text{out}}} \mathbf{g} \cdot \mathbf{v}_h, \end{aligned} \quad (4)$$

for all $(\mathbf{v}_h, q_h, \mathbf{w}_h, \dot{\mathbf{w}}_h) \in V_h \times Q_h \times X_h \times X_h$. Here, $\bar{\mathbf{u}}_h$ stands for a suitable interpolation of the boundary data $\bar{\mathbf{u}}$ on Γ^{in} , α for a given parameter taking values in $\{-1, 1\}$, and $\gamma > 0$ for the Nitsche's penalty parameter. Moreover, the

fluid and solid (volumic) bi-linear forms are given by

$$A^f((\mathbf{u}_h, p_h), (\mathbf{v}_h, q_h)) \stackrel{\text{def}}{=} \rho^f \int_{\Omega^f} \partial_t \mathbf{u}_h \cdot \mathbf{v}_h + \int_{\Omega^f} \boldsymbol{\sigma}(\mathbf{u}_h, p_h) : \boldsymbol{\epsilon}(\mathbf{v}_h) + \int_{\Omega^f} q_h \nabla \cdot \mathbf{u}_h,$$

$$A^s((\boldsymbol{\eta}_h, \dot{\boldsymbol{\eta}}_h), (\mathbf{w}_h, \dot{\mathbf{w}}_h)) \stackrel{\text{def}}{=} \rho^s \int_{\Omega^s} \partial_t \dot{\boldsymbol{\eta}}_h \cdot \mathbf{w}_h + a^s(\boldsymbol{\eta}_h, \mathbf{w}_h) + \int_{\Omega^s} (\dot{\boldsymbol{\eta}}_h - \partial_t \boldsymbol{\eta}_h) \cdot \dot{\mathbf{w}}_h,$$

where a^s stands for a general solid stiffness symmetric bi-linear form.

Note the boundary integrations on Σ , these are the Nitsche's weak coupling terms. The interface integrals involving the stress tensor $\boldsymbol{\sigma}$ are computed face-wise, as broken integrals. Let us emphasize that the approximation in each subdomain (fluid and structure) involves standard conforming finite element spaces, with strongly imposed Dirichlet boundary conditions on Γ^{in} and Γ^{d} . Only the interface coupling conditions (3) are treated using Nitsche's method. In particular, the functions of V_h and X_h do not necessarily match at the interface Σ , which leads to the interface integrals in (4). This differs from classic fluid-structure formulations (see *e.g.* [25]), where interface integrals cancel due to the strong enforcement of the kinematic condition (3)₁.

Remark 3.1 *The parameter α characterizes the type of formulation: symmetric ($\alpha = 1$) or non-symmetric ($\alpha = -1$). The former is often preferred, for instance, in order to derive optimal L^2 -error estimates for the fluid velocity (using the Aubin-Nitsche's duality trick). Note that the Nitsche's formulation (4) differs from the one proposed in [21], within a space-time framework. Indeed, in [21], the symmetrizing (consistent) coupling term is given by $\int_{\Sigma} (\mathbf{u}_h - \partial_t \boldsymbol{\eta}_h) \cdot \boldsymbol{\sigma}(\mathbf{v}_h, q_h) \mathbf{n}$, instead of $\int_{\Sigma} (\mathbf{u}_h - \partial_t \boldsymbol{\eta}_h) \cdot \boldsymbol{\sigma}(\alpha \mathbf{v}_h, -q_h) \mathbf{n}$, as we propose in (4).*

Remark 3.2 *As noticed in [3, 19], the first coupling term in (4)₃, involving the fluid stresses on the interface, could be replaced by any convex combination of the fluid and solid interface stresses, namely,*

$$\beta \boldsymbol{\sigma}(\mathbf{u}_h, p_h) \mathbf{n} + (1 - \beta) \boldsymbol{\sigma}(\boldsymbol{\eta}_h) \mathbf{n}, \quad \beta \in [0, 1].$$

Here, for stability purposes (see Section 5), we have chosen a fluid-sided "mortaring", i.e. we take $\beta = 1$.

3.1 Stability

In what follows, we shall make use of the following trace-inverse inequality (see *e.g.* [39])

$$\|\mathbf{v}_h\|_{0, \partial K}^2 \leq C_{\text{TI}} h^{-1} \|\mathbf{v}_h\|_{0, K}^2, \quad \forall \mathbf{v}_h \in W_h, \quad (5)$$

for all $K \in \mathcal{T}_h^f$.

The following Lemma provides an *a priori* energy stability estimate for the semi-discrete formulation (4).

Lemma 3.3 *Assume that the fluid-structure system is isolated, i.e. $\bar{\mathbf{u}} = \mathbf{0}$ and $\mathbf{g} = \mathbf{0}$. Let $(\mathbf{u}_h, p_h, \boldsymbol{\eta}_h, \dot{\boldsymbol{\eta}}_h)$ the solution of (4). Then, under the condition*

$$\gamma > 8(1 + \alpha)C_{\text{TI}}, \quad (6)$$

the following energy estimate holds,

$$\begin{aligned} & \frac{\rho^f}{2} \|\mathbf{u}_h\|_{0,\Omega^f}^2 + \frac{\rho^s}{2} \|\dot{\boldsymbol{\eta}}_h\|_{0,\Omega^s}^2 + \frac{1}{2} a^s(\boldsymbol{\eta}_h, \boldsymbol{\eta}_h) + \frac{\mu}{2} \int_0^t \|\boldsymbol{\epsilon}(\mathbf{u}_h)\|_{0,\Omega^f}^2 \\ & + \frac{\gamma\mu}{2h} \int_0^t \|\mathbf{u}_h - \partial_t \boldsymbol{\eta}_h\|_{0,\Sigma}^2 \leq \frac{\rho^f}{2} \|\mathbf{u}_h^0\|_{0,\Omega^f}^2 + \frac{\rho^s}{2} \|\dot{\boldsymbol{\eta}}_h^0\|_{0,\Omega^s}^2 + \frac{1}{2} a^s(\boldsymbol{\eta}_h^0, \boldsymbol{\eta}_h^0). \end{aligned} \quad (7)$$

In particular, for $\alpha = -1$ this estimate holds true for all values of the Nitsche's penalty parameter $\gamma > 0$.

Proof. By taking

$$(\mathbf{v}_h, q_h, \mathbf{w}_h, \dot{\mathbf{w}}_h) = (\mathbf{u}_h, p_h, \partial_t \boldsymbol{\eta}_h, \partial_t \dot{\boldsymbol{\eta}}_h),$$

in (4) we have ,

$$\begin{aligned} & \frac{d}{dt} \left(\frac{\rho^f}{2} \|\mathbf{u}_h\|_{0,\Omega^f}^2 + \frac{\rho^s}{2} \|\dot{\boldsymbol{\eta}}_h\|_{0,\Omega^s}^2 + \frac{1}{2} a^s(\boldsymbol{\eta}_h, \boldsymbol{\eta}_h) \right) + \mu \|\boldsymbol{\epsilon}(\mathbf{u}_h)\|_{0,\Omega^f}^2 \\ & + \frac{\gamma\mu}{h} \|\mathbf{u}_h - \partial_t \boldsymbol{\eta}_h\|_{0,\Sigma}^2 - 2(1 + \alpha)\mu \int_{\Sigma} \boldsymbol{\epsilon}(\mathbf{u}_h) \mathbf{n} \cdot (\mathbf{u}_h - \partial_t \boldsymbol{\eta}_h) = 0. \end{aligned} \quad (8)$$

On the other hand, using the trace-inverse inequality (5) and since $|\alpha| = 1$, we obtain

$$\begin{aligned} -2(1 + \alpha)\mu \int_{\Sigma} \boldsymbol{\epsilon}(\mathbf{u}_h) \mathbf{n} \cdot (\mathbf{u}_h - \partial_t \boldsymbol{\eta}_h) & \leq \frac{4(1 + \alpha)\mu C_{\text{TI}}}{\gamma} \|\boldsymbol{\epsilon}(\mathbf{u}_h)\|_{0,\Omega^f}^2 \\ & + \frac{\gamma\mu}{2h} \|\mathbf{u}_h - \partial_t \boldsymbol{\eta}_h\|_{0,\Sigma}^2. \end{aligned} \quad (9)$$

Thus, inserting this expression in (8) and after integration over $(0, t)$, we have

$$\begin{aligned} & \frac{\rho^f}{2} \|\mathbf{u}_h(t)\|_{0,\Omega^f}^2 + \frac{\rho^s}{2} \|\dot{\boldsymbol{\eta}}_h\|_{0,\Omega^s}^2 + \frac{1}{2} a^s(\boldsymbol{\eta}_h, \boldsymbol{\eta}_h) + \mu_{\alpha} \int_0^t \|\boldsymbol{\epsilon}(\mathbf{u}_h)\|_{0,\Omega^f}^2 \\ & + \frac{\gamma\mu}{2h} \int_0^t \|\mathbf{u}_h - \partial_t \boldsymbol{\eta}_h\|_{0,\Sigma}^2 \leq \frac{\rho^f}{2} \|\mathbf{u}_h^0\|_{0,\Omega^f}^2 + \frac{\rho^s}{2} \|\dot{\boldsymbol{\eta}}_h^0\|_{0,\Omega^s}^2 + \frac{1}{2} a^s(\boldsymbol{\eta}_h^0, \boldsymbol{\eta}_h^0), \end{aligned}$$

with

$$\mu_{\alpha} \stackrel{\text{def}}{=} \mu \left(1 - \frac{4(1 + \alpha)C_{\text{TI}}}{\gamma} \right),$$

which completes the proof. \square

Note that the (additional) interface term in the energy inequality (7) appears due to the dissipative character of the Nitsche's coupling.

3.2 Partitioned formulation

In this paper we focus on *partitioned* procedures for the numerical resolution of the monolithic (or global) formulation (4), *i.e.* methods which only involve separate solutions of the fluid and structure sub-problems (1) and (2) (with appropriate boundary conditions on Σ). Such procedures enable the design of efficient fluid-structure solution algorithms, while keeping state-of-the-art methods and software in each sub-domain (see *e.g.* [32, 12, 28, 18, 14, 15, 13]).

To this aim, we reformulate problem (4) in terms of two coupled problems. This can be achieved by simply taking $(\mathbf{v}_h, q_h) = (\mathbf{0}, 0)$ or $\mathbf{w}_h = \dot{\mathbf{w}}_h = \mathbf{0}$ in (4), which yields:

- **Solid sub-problem:** Given $(\mathbf{u}_h, p_h) \in W_h \times Q_h$, find $(\boldsymbol{\eta}_h, \dot{\boldsymbol{\eta}}_h) \in X_h \times X_h$ such that

$$\begin{aligned} A^s((\boldsymbol{\eta}_h, \dot{\boldsymbol{\eta}}_h), (\mathbf{w}_h, \dot{\mathbf{w}}_h)) + \gamma \frac{\mu}{h} \int_{\Sigma} \partial_t \boldsymbol{\eta}_h \cdot \mathbf{w}_h \\ = \gamma \frac{\mu}{h} \int_{\Sigma} \mathbf{u}_h \cdot \mathbf{w}_h - \int_{\Sigma} \boldsymbol{\sigma}(\mathbf{u}_h, p_h) \mathbf{n} \cdot \mathbf{w}_h, \end{aligned} \quad (10)$$

for all $(\mathbf{w}_h, \dot{\mathbf{w}}_h) \in X_h \times X_h$.

- **Fluid sub-problem:** Given $\boldsymbol{\eta}_h \in X_h$, find $(\mathbf{u}_h, p_h) \in W_h \times Q_h$, with $\mathbf{u}_h = \bar{\mathbf{u}}_h$ on Γ^{in} , such that

$$\begin{aligned} A^f((\mathbf{u}_h, p_h), (\mathbf{v}_h, q_h)) - \int_{\Sigma} \boldsymbol{\sigma}(\mathbf{u}_h, p_h) \mathbf{n} \cdot \mathbf{v}_h - \int_{\Sigma} \mathbf{u}_h \cdot \boldsymbol{\sigma}(\alpha \mathbf{v}_h, -q_h) \mathbf{n} + \gamma \frac{\mu}{h} \int_{\Sigma} \mathbf{u}_h \cdot \mathbf{v}_h \\ = - \int_{\Sigma} \partial_t \boldsymbol{\eta}_h \cdot \boldsymbol{\sigma}(\alpha \mathbf{v}_h, -q_h) \mathbf{n} + \gamma \frac{\mu}{h} \int_{\Sigma} \partial_t \boldsymbol{\eta}_h \cdot \mathbf{v}_h + \int_{\Gamma^{\text{out}}} \mathbf{g} \cdot \mathbf{v}_h, \end{aligned} \quad (11)$$

for all $(\mathbf{v}_h, q_h) \in V_h \times Q_h$.

From the numerical point of view, the discrete solid sub-problem (10) corresponds to the finite element approximation of the structural mechanics sub-problem (2)₁, with the following Robin-type boundary conditions on the interface:

$$\boldsymbol{\sigma}^s(\boldsymbol{\eta}) \mathbf{n} - \gamma \frac{\mu}{h} \partial_t \boldsymbol{\eta} = \boldsymbol{\sigma}(\mathbf{u}, p) \mathbf{n} - \gamma \frac{\mu}{h} \mathbf{u}, \quad \text{on } \Sigma. \quad (12)$$

On the other hand, the fluid sub-problem (11) is nothing but the finite element approximation of the fluid mechanics sub-problem (1), with the following Dirichlet condition

$$\mathbf{u} = \partial_t \boldsymbol{\eta}, \quad \text{on } \Sigma, \quad (13)$$

weakly enforced using Nitsche's method.

In summary, the fluid-structure Nitsche's formulation (4) can be reformulated, in a partitioned fashion, as two sub-problems (structure and fluid) coupled through Robin, (12), and Dirichlet-Nitsche, (13), transmission conditions. This is in contrast with the traditional Dirichlet-Neumann formulation, where only forces are transferred from the fluid to the solid (see *e.g.* [25, 26, 18, 15]). We refer also to the recent work [1], where the coupling is prescribed in terms of Robin-Robin conditions, in order to accelerate the convergence of a partitioned solution procedure (within the context of an implicit coupling scheme).

Remark 3.4 *In the traditional fluid-structure formulations (in which V_h and X_h match at the interface, up to interpolation), stability requires (at least theoretically, see *e.g.* [25]) the interface fluid force to be given as the fluid-subproblem variational residual. In the solid-subproblem (10) of the Nitsche's formulation (4), on the contrary, no such a variational consistency is needed to ensure stability. The interface fluid force is simply given as an interface integral. This will be crucial, in section §5, to stabilize a fluid-structure explicit coupling scheme.*

4 Time discretization: coupling strategies

For the time discretization we propose to replace all time derivatives in (10)-(11) by backward differences. Let $(0, T)$ be the time interval of interest. For a given integer $N \in \mathbb{N}^*$, we introduce the time-step $\delta t \stackrel{\text{def}}{=} T/N$ and the time grid $t_n \stackrel{\text{def}}{=} n\delta t$, with $0 \leq n \leq N$. In what follows, we will use the following general notation for the first order backward difference $\partial_{\delta t} X^{n+1} \stackrel{\text{def}}{=} \delta t^{-1}(X^{n+1} - X^n)$.

We consider a first order backward difference discretization in the fluid and a Newmark's scheme for the structure, so that the fully discrete fluid and solid bi-linear forms are given by:

$$\begin{aligned} A_{\delta t}^f((\mathbf{u}_h^{n+1}, p_h^{n+1}), (\mathbf{v}_h, q_h)) &\stackrel{\text{def}}{=} \rho^f \int_{\Omega^f} \partial_{\delta t} \mathbf{u}_h^{n+1} \cdot \mathbf{v}_h + \int_{\Omega^f} \boldsymbol{\sigma}(\mathbf{u}_h^{n+1}, p_h^{n+1}) : \boldsymbol{\epsilon}(\mathbf{v}_h) \\ &\quad + \int_{\Omega^f} q_h \nabla \cdot \mathbf{u}_h^{n+1}, \\ A_{\delta t}^s((\boldsymbol{\eta}_h^{n+1}, \dot{\boldsymbol{\eta}}_h^{n+1}), (\mathbf{w}_h, \dot{\mathbf{w}}_h)) &\stackrel{\text{def}}{=} \rho^s \int_{\Omega^s} \partial_{\delta t} \dot{\boldsymbol{\eta}}_h^{n+1} \cdot \mathbf{w}_h + \frac{1}{2} a^s(\boldsymbol{\eta}_h^{n+1} + \boldsymbol{\eta}_h^n, \mathbf{w}_h) \\ &\quad + \int_{\Omega^s} \left(\frac{\dot{\boldsymbol{\eta}}_h^{n+1} + \dot{\boldsymbol{\eta}}_h^n}{2} - \partial_{\delta t} \boldsymbol{\eta}_h^{n+1} \right) \cdot \dot{\mathbf{w}}_h, \end{aligned}$$

As a result, the fully discrete partitioned fluid-structure formulation is given by:

- **Solid sub-problem:** Given $(\mathbf{u}_h^*, p_h^*) \in W_h \times Q_h$, find $(\boldsymbol{\eta}_h^{n+1}, \dot{\boldsymbol{\eta}}_h^{n+1}) \in X_h \times X_h$ such that

$$\begin{aligned} A_{\delta t}^s((\boldsymbol{\eta}_h^{n+1}, \dot{\boldsymbol{\eta}}_h^{n+1}), (\mathbf{w}_h, \dot{\mathbf{w}}_h)) + \gamma \frac{\mu}{h} \int_{\Sigma} \partial_{\delta t} \boldsymbol{\eta}_h^{n+1} \cdot \mathbf{w}_h \\ = \gamma \frac{\mu}{h} \int_{\Sigma} \mathbf{u}_h^* \cdot \mathbf{w}_h - \int_{\Sigma} \boldsymbol{\sigma}(\mathbf{u}_h^*, p_h^*) \mathbf{n} \cdot \mathbf{w}_h, \end{aligned} \quad (14)$$

for all $(\mathbf{w}_h, \dot{\mathbf{w}}_h) \in X_h \times X_h$.

- **Fluid sub-problem:** Given $\partial_{\delta t} \boldsymbol{\eta}_h^{n+1} \in X_h$, find $(\mathbf{u}_h^{n+1}, p_h^{n+1}) \in W_h \times Q_h$, with $\mathbf{u}_h^{n+1} = \bar{\mathbf{u}}_h(t_{n+1})$ on Γ^{in} , such that

$$\begin{aligned} A_{\delta t}^f((\mathbf{u}_h^{n+1}, p_h^{n+1}), (\mathbf{v}_h, q_h)) - \int_{\Sigma} \boldsymbol{\sigma}(\mathbf{u}_h^{n+1}, p_h^{n+1}) \mathbf{n} \cdot \mathbf{v}_h - \int_{\Sigma} \mathbf{u}_h^{n+1} \cdot \boldsymbol{\sigma}(\alpha \mathbf{v}_h, -q_h) \mathbf{n} \\ + \gamma \frac{\mu}{h} \int_{\Sigma} \mathbf{u}_h^{n+1} \cdot \mathbf{v}_h = - \int_{\Sigma} \partial_{\delta t} \boldsymbol{\eta}_h^{n+1} \cdot \boldsymbol{\sigma}(\alpha \mathbf{v}_h, -q_h) \mathbf{n} + \gamma \frac{\mu}{h} \int_{\Sigma} \partial_{\delta t} \boldsymbol{\eta}_h^{n+1} \cdot \mathbf{v}_h \\ + \int_{\Gamma^{\text{out}}} \mathbf{g}(t_{n+1}) \cdot \mathbf{v}_h, \end{aligned} \quad (15)$$

for all $(\mathbf{v}_h, q_h) \in V_h \times Q_h$.

If $\mathbf{u}_h^* \stackrel{\text{def}}{=} \mathbf{u}_h^{n+1}$ and $p_h^* \stackrel{\text{def}}{=} p_h^{n+1}$ for $0 \leq n \leq N-1$, the scheme (14)-(15) corresponds to an implicit coupling scheme. On the other hand, if $\mathbf{u}_h^* \stackrel{\text{def}}{=} \mathbf{u}_h^n$ and $p_h^* \stackrel{\text{def}}{=} p_h^n$ for $0 \leq n \leq N-1$, the scheme is (fully) explicit or *loosely coupled*.

In the next two paragraphs, we will discuss the stability properties of the numerical schemes resulting from these choices of \mathbf{u}_h^* and p_h^* . In Section §5, we will show that the explicit coupling scheme can be stabilized by adding, to the fluid sub-problem, a suitable interface time-penalization term.

4.1 Implicit coupling

For $\mathbf{u}_h^* = \mathbf{u}_h^{n+1}$ and $p_h^* = p_h^{n+1}$, $0 \leq n \leq N-1$, the scheme (14)-(15) corresponds to an implicit coupling scheme. In other words, at each time level, n , the sub-problems (14) and (15) are fully coupled.

By adding (14) and (15), the implicit scheme can be reformulated (monolithically) as follows: Find $(\mathbf{u}_h^{n+1}, p_h^{n+1}, \boldsymbol{\eta}_h^{n+1}, \dot{\boldsymbol{\eta}}_h^{n+1}) \in W_h \times Q_h \times X_h \times X_h$, with $\mathbf{u}_h^{n+1} = \bar{\mathbf{u}}_h(t_{n+1})$ on Γ^{in} , such that

$$\begin{aligned} & A_{\delta t}^f((\mathbf{u}_h^{n+1}, p_h^{n+1}), (\mathbf{v}_h, q_h)) + A_{\delta t}^s((\boldsymbol{\eta}_h^{n+1}, \dot{\boldsymbol{\eta}}_h^{n+1}), (\mathbf{w}_h, \dot{\mathbf{w}}_h)) \\ & - \int_{\Sigma} \boldsymbol{\sigma}(\mathbf{u}_h^{n+1}, p_h^{n+1}) \mathbf{n} \cdot (\mathbf{v}_h - \mathbf{w}_h) - \int_{\Sigma} (\mathbf{u}_h^{n+1} - \partial_{\delta t} \boldsymbol{\eta}_h^{n+1}) \cdot \boldsymbol{\sigma}(\alpha \mathbf{v}_h, -q_h) \mathbf{n} \\ & + \gamma \frac{\mu}{h} \int_{\Sigma} (\mathbf{u}_h^{n+1} - \partial_t \boldsymbol{\eta}_h^{n+1}) \cdot (\mathbf{v}_h - \mathbf{w}_h) = \int_{\Gamma^{\text{out}}} \mathbf{g}(t_{n+1}) \cdot \mathbf{v}_h, \end{aligned} \quad (16)$$

for all $(\mathbf{v}_h, q_h, \mathbf{w}_h, \dot{\mathbf{w}}_h) \in V_h \times Q_h \times X_h \times X_h$, which is a fully discrete counterpart of (4).

In order to simplify the presentation, we introduce the following notations: $\mathbf{U}_h^{n+1} \stackrel{\text{def}}{=} (\mathbf{u}_h^{n+1}, p_h^{n+1})$ and $\mathbf{V}_h \stackrel{\text{def}}{=} (\mathbf{v}_h, q_h)$ stand for the fluid state and test functions, $\boldsymbol{\Theta}_h^{n+1} \stackrel{\text{def}}{=} (\boldsymbol{\eta}_h^{n+1}, \dot{\boldsymbol{\eta}}_h^{n+1})$ and $\mathbf{W}_h \stackrel{\text{def}}{=} (\mathbf{w}_h, \dot{\mathbf{w}}_h)$ for the solid state and test functions and

$$\begin{aligned} A_I[(\mathbf{U}_h^{n+1}, \boldsymbol{\Theta}_h^{n+1}), (\mathbf{V}_h, \mathbf{W}_h)] & \stackrel{\text{def}}{=} A_{\delta t}^f((\mathbf{u}_h^{n+1}, p_h^{n+1}), (\mathbf{v}_h, q_h)) \\ & + A_{\delta t}^s((\boldsymbol{\eta}_h^{n+1}, \dot{\boldsymbol{\eta}}_h^{n+1}), (\mathbf{w}_h, \dot{\mathbf{w}}_h)) \\ & - \int_{\Sigma} \boldsymbol{\sigma}(\mathbf{u}_h^{n+1}, p_h^{n+1}) \mathbf{n} \cdot (\mathbf{v}_h - \mathbf{w}_h) \\ & - \int_{\Sigma} (\mathbf{u}_h^{n+1} - \partial_{\delta t} \boldsymbol{\eta}_h^{n+1}) \cdot \boldsymbol{\sigma}(\alpha \mathbf{v}_h, -q_h) \mathbf{n} \\ & + \gamma \frac{\mu}{h} \int_{\Sigma} (\mathbf{u}_h^{n+1} - \partial_t \boldsymbol{\eta}_h^{n+1}) \cdot (\mathbf{v}_h - \mathbf{w}_h). \end{aligned} \quad (17)$$

for the implicit coupling bi-linear form. As a result, (16) simply reduces to

$$A_I[(\mathbf{U}_h^{n+1}, \boldsymbol{\Theta}_h^{n+1}), (\mathbf{V}_h, \mathbf{W}_h)] = \int_{\Gamma^{\text{out}}} \mathbf{g}(t_{n+1}) \cdot \mathbf{v}_h, \quad (18)$$

for all $(\mathbf{V}_h, \mathbf{W}_h) \in (V_h \times Q_h) \times X_h^2$.

4.1.1 Stability analysis – implicit coupling

As one could expect, implicit coupling is unconditionally stable in the energy norm. Let E^n denote the total discrete energy of the system at the time level

n , defined by

$$\begin{aligned} E^n \stackrel{\text{def}}{=} & \frac{\rho^f}{2} \|\mathbf{u}_h^n\|_{0,\Omega^f}^2 + \frac{\rho^s}{2} \|\dot{\boldsymbol{\eta}}_h^n\|_{0,\Omega^s}^2 + \frac{1}{2} a^s(\boldsymbol{\eta}_h^n, \boldsymbol{\eta}_h^n) + \delta t \frac{\mu}{2} \sum_{m=0}^{n-1} \|\boldsymbol{\epsilon}(\mathbf{u}_h^{m+1})\|_{0,\Omega^f}^2 \\ & + \delta t \frac{\gamma\mu}{2h} \sum_{m=0}^{n-1} \|\mathbf{u}_h^{m+1} - \partial_t \boldsymbol{\eta}_h^{m+1}\|_{0,\Sigma}^2. \end{aligned} \quad (19)$$

The next Lemma states the unconditional stability of the implicit coupling scheme, (14)-(15) with $\mathbf{u}_h^* \stackrel{\text{def}}{=} \mathbf{u}_h^{n+1}$ and $p_h^* \stackrel{\text{def}}{=} p_h^{n+1}$.

Lemma 4.1 *Assume that the fluid-structure system is isolated, i.e. $\bar{\mathbf{u}} = \mathbf{0}$ and $\mathbf{g} = \mathbf{0}$. Let $\{(\mathbf{u}_h^{n+1}, p_h^{n+1}, \boldsymbol{\eta}_h^{n+1}, \dot{\boldsymbol{\eta}}_h^{n+1})\}_{0 \leq n \leq N-1}$ the solution of (14)-(15) with $\mathbf{u}_h^* \stackrel{\text{def}}{=} \mathbf{u}_h^{n+1}$ and $p_h^* \stackrel{\text{def}}{=} p_h^{n+1}$. Then, under the condition (6), the following energy estimate holds,*

$$E^n \leq E^0,$$

with $1 \leq n \leq N - 1$. In particular, for $\alpha = -1$ this estimate holds true for all values of the Nitsche's penalty parameter $\gamma > 0$.

Proof. The proof follows, with minor modifications, the proof of Lemma 3.3 for the space semi-discrete case. Indeed, by testing (18) with

$$(\mathbf{v}_h, q_h, \mathbf{w}_h, \dot{\mathbf{w}}_h) = (\mathbf{u}_h^{n+1}, p_h^{n+1}, \partial_{\delta t} \boldsymbol{\eta}_h^{n+1}, \partial_{\delta t} \dot{\boldsymbol{\eta}}_h^{n+1}),$$

using (9), summing over n , using condition (6) and the definition (19), we get

$$E^n \leq \frac{\rho^f}{2} \|\mathbf{u}_h^0\|_{0,\Omega^f}^2 + \frac{\rho^s}{2} \|\dot{\boldsymbol{\eta}}_h^0\|_{0,\Omega^s}^2 + \frac{1}{2} a^s(\boldsymbol{\eta}_h^0, \boldsymbol{\eta}_h^0),$$

which completes the proof. \square

Despite the outstanding stability properties provided by the previous Lemma, implicit coupling has the major disadvantage of being too CPU-time consuming. Indeed, at each time-level n , it involves the solution of the fully coupled system (18), which can be solved monolithically, by treating (18) as an individual problem, or in a partitioned fashion, by sub-iterating (until convergence!) between the fluid and solid subproblems (14)-(15).

4.2 Explicit coupling

For $\mathbf{u}_h^* = \mathbf{u}_h^n$ and $p_h^* = p_h^n$, $0 \leq n \leq N - 1$, the scheme (14)-(15) is explicit (or loosely coupled). In such a procedure, one can advance in time by solving first for the solid in (14), since (\mathbf{u}_h^n, p_h^n) is known from the previous time level, and then for the fluid in (15), since $\partial_{\delta t} \boldsymbol{\eta}_h^{n+1}$ is provided by the previous solid step. This simple splitting procedure, for solving fluid-structure interaction problems, is also known in the literature as conventional serial staggered (CSS) scheme (see e.g. [32, 12]).

Clearly, explicit coupling is very appealing in terms of efficiency: it only involves one (or a few) solution of the fluid and solid sub-problems per time step. However, this fluid-solid splitting can drastically compromise the numerical stability of the scheme, as showed in [7, 17], when dealing with incompressible fluids.

To illustrate this issue, in the case of the partitioned Nitsche fluid-structure formulation (14)-(15), we reformulate the explicit coupling scheme in a monolithic fashion, as we did for the implicit scheme in (18), by adding the expressions (14) and (15). This yields the global problem: Find $(\mathbf{u}_h^{n+1}, p_h^{n+1}, \boldsymbol{\eta}_h^{n+1}, \dot{\boldsymbol{\eta}}_h^{n+1}) \in W_h \times Q_h \times X_h \times X_h$, with $\mathbf{u}_h^{n+1} = \bar{\mathbf{u}}_h(t_{n+1})$ on Γ^{in} , such that

$$\begin{aligned} & A_{\delta t}^f((\mathbf{u}_h^{n+1}, p_h^{n+1}), (\mathbf{v}_h, q_h)) + A_{\delta t}^s((\boldsymbol{\eta}_h^{n+1}, \dot{\boldsymbol{\eta}}_h^{n+1}), (\mathbf{w}_h, \dot{\mathbf{w}}_h)) - \int_{\Sigma} \boldsymbol{\sigma}(\mathbf{u}_h^{n+1}, p_h^{n+1}) \mathbf{n} \cdot \mathbf{v}_h \\ & + \int_{\Sigma} \boldsymbol{\sigma}(\mathbf{u}_h^n, p_h^n) \mathbf{n} \cdot \mathbf{w}_h - \int_{\Sigma} (\mathbf{u}_h^{n+1} - \partial_{\delta t} \boldsymbol{\eta}_h^{n+1}) \cdot \boldsymbol{\sigma}(\alpha \mathbf{v}_h, -q_h) \mathbf{n} \\ & + \gamma \frac{\mu}{h} \int_{\Sigma} (\mathbf{u}_h^{n+1} - \partial_t \boldsymbol{\eta}_h^{n+1}) \cdot \mathbf{v}_h - \gamma \frac{\mu}{h} \int_{\Sigma} (\mathbf{u}_h^n - \partial_t \boldsymbol{\eta}_h^{n+1}) \cdot \mathbf{w}_h = \int_{\Gamma^{\text{out}}} \mathbf{g}(t_{n+1}) \cdot \mathbf{v}_h, \end{aligned} \quad (20)$$

for all $(\mathbf{v}_h, q_h, \mathbf{w}_h, \dot{\mathbf{w}}_h) \in V_h \times Q_h \times X_h \times X_h$, which is an explicit coupling fully discrete counterpart of (4). Equivalently, in a more compact form,

$$A_E[(\mathbf{U}_h^{n+1}, \boldsymbol{\Theta}_h^{n+1}), (\mathbf{V}_h, \mathbf{W}_h)] = \int_{\Gamma^{\text{out}}} \mathbf{g}^{n+1} \cdot \mathbf{v}_h, \quad (21)$$

for all $(\mathbf{V}_h, \mathbf{W}_h) \in (V_h \times Q_h) \times X_h^2$, where the explicit bi-linear form A_E is given by

$$\begin{aligned} A_E[(\mathbf{U}_h^{n+1}, \boldsymbol{\Theta}_h^{n+1}), (\mathbf{V}_h, \mathbf{W}_h)] & \stackrel{\text{def}}{=} A_{\delta t}^f((\mathbf{u}_h^{n+1}, p_h^{n+1}), (\mathbf{v}_h, q_h)) \\ & + A_{\delta t}^s((\boldsymbol{\eta}_h^{n+1}, \dot{\boldsymbol{\eta}}_h^{n+1}), (\mathbf{w}_h, \dot{\mathbf{w}}_h)) \\ & - \int_{\Sigma} \boldsymbol{\sigma}(\mathbf{u}_h^{n+1}, p_h^{n+1}) \mathbf{n} \cdot \mathbf{v}_h + \int_{\Sigma} \boldsymbol{\sigma}(\mathbf{u}_h^n, p_h^n) \mathbf{n} \cdot \mathbf{w}_h \\ & - \int_{\Sigma} (\mathbf{u}_h^{n+1} - \partial_{\delta t} \boldsymbol{\eta}_h^{n+1}) \cdot \boldsymbol{\sigma}(\alpha \mathbf{v}_h, -q_h) \mathbf{n} \\ & + \gamma \frac{\mu}{h} \int_{\Sigma} (\mathbf{u}_h^{n+1} - \partial_t \boldsymbol{\eta}_h^{n+1}) \cdot \mathbf{v}_h \\ & - \gamma \frac{\mu}{h} \int_{\Sigma} (\mathbf{u}_h^n - \partial_t \boldsymbol{\eta}_h^{n+1}) \cdot \mathbf{w}_h. \end{aligned}$$

From (17), it then follows that

$$\begin{aligned} A_E[(\mathbf{U}_h^{n+1}, \boldsymbol{\Theta}_h^{n+1}), (\mathbf{V}_h, \mathbf{W}_h)] & = A_I[(\mathbf{U}_h^{n+1}, \boldsymbol{\Theta}_h^{n+1}), (\mathbf{V}_h, \mathbf{W}_h)] \\ & + \gamma \frac{\mu}{h} \int_{\Sigma} (\mathbf{u}_h^{n+1} - \mathbf{u}_h^n) \cdot \mathbf{w}_h \\ & - \int_{\Sigma} (\boldsymbol{\sigma}(\mathbf{u}_h^{n+1}, p_h^{n+1}) \mathbf{n} - \boldsymbol{\sigma}(\mathbf{u}_h^n, p_h^n) \mathbf{n}) \cdot \mathbf{w}_h. \end{aligned} \quad (22)$$

Therefore, the explicit coupling scheme can be thought of as an interface perturbation of the implicit coupling scheme. This perturbation consists of two terms, related to the time variations of the fluid velocity and fluid stresses at the interface Σ . In the next paragraph we will see that the dissipative character of the Nitsche's coupling is able to control the first perturbation, under a suitable CFL-like condition (see Remark 5.4). The second, on the contrary, needs a special treatment, which will be topic of Section §5.

4.2.1 Stability analysis – explicit coupling

Let us stress that the purpose of this paragraph is simply to illustrate (not to prove) the instability of the explicit coupling scheme (14)-(15). The discussion below will motivate the introduction of a new (stabilized) explicit coupling scheme in Section §5.

Lemma 4.2 *Assume that the fluid-structure system is isolated, i.e. $\bar{\mathbf{u}} = \mathbf{0}$ and $\mathbf{g} = \mathbf{0}$. Let $\{(\mathbf{u}_h^{n+1}, p_h^{n+1}, \boldsymbol{\eta}_h^{n+1}, \dot{\boldsymbol{\eta}}_h^{n+1})\}_{0 \leq n \leq N-1}$ the solution of (14)-(15) with $\mathbf{u}_h^* \stackrel{\text{def}}{=} \mathbf{u}_h^n$ and $p_h^* \stackrel{\text{def}}{=} p_h^n$. Then, under the conditions (6) and*

$$\delta t \leq \frac{C_\Sigma}{\gamma\mu} h, \quad (23)$$

with $C_\Sigma > 0$ a given constant, the following estimate holds,

$$\begin{aligned} E^n + \delta t \frac{\gamma\mu}{h} \|\mathbf{u}_h^n\|_{0,\Sigma}^2 &\leq 2E^0 + C_\Sigma \|\mathbf{u}_h^0\|_{0,\Sigma}^2 \\ &\quad - 2\delta t \sum_{m=0}^{n-1} \int_{\Sigma} (\boldsymbol{\sigma}(\mathbf{u}_h^{m+1}, p_h^{m+1}) \mathbf{n} - \boldsymbol{\sigma}(\mathbf{u}_h^m, p_h^m) \mathbf{n}) \cdot \partial_{\delta t} \boldsymbol{\eta}_h^{m+1}. \end{aligned} \quad (24)$$

Proof. By testing (21) with

$$(\mathbf{v}_h, q_h, \mathbf{w}_h, \dot{\mathbf{w}}_h) = (\mathbf{u}_h^{n+1}, p_h^{n+1}, \partial_{\delta t} \boldsymbol{\eta}_h^{n+1}, \partial_{\delta t} \dot{\boldsymbol{\eta}}_h^{n+1}),$$

using (22), multiplying by δt , summing over $0 \leq m \leq n-1$ and using the stability analysis of the implicit scheme, we have

$$\begin{aligned} E^n &\leq E^0 - \underbrace{\delta t \frac{\gamma\mu}{h} \sum_{m=0}^{n-1} \int_{\Sigma} (\mathbf{u}_h^{m+1} - \mathbf{u}_h^m) \cdot \partial_{\delta t} \boldsymbol{\eta}_h^{m+1}}_{T_1} \\ &\quad + \delta t \sum_{m=0}^{n-1} \int_{\Sigma} (\boldsymbol{\sigma}(\mathbf{u}_h^{m+1}, p_h^{m+1}) \mathbf{n} - \boldsymbol{\sigma}(\mathbf{u}_h^m, p_h^m) \mathbf{n}) \cdot \partial_{\delta t} \boldsymbol{\eta}_h^{m+1}. \end{aligned} \quad (25)$$

As mentioned above, the term T_1 involving the fluid velocity fluctuations at the interface can be handled using the Nitsche's penalty coupling term. Indeed, we have

$$\begin{aligned} T_1 &= \delta t \frac{\gamma\mu}{h} \sum_{m=0}^{n-1} \int_{\Sigma} (\mathbf{u}_h^{m+1} - \mathbf{u}_h^m) \cdot (\mathbf{u}_h^{m+1} + \partial_{\delta t} \boldsymbol{\eta}_h^{m+1} - \mathbf{u}_h^{m+1}) \\ &= \delta t \frac{\gamma\mu}{h} \sum_{m=0}^{n-1} \left[\int_{\Sigma} (\mathbf{u}_h^{m+1} - \mathbf{u}_h^m) \cdot \mathbf{u}_h^{m+1} - \int_{\Sigma} (\mathbf{u}_h^{m+1} - \mathbf{u}_h^m) \cdot (\mathbf{u}_h^{m+1} - \partial_{\delta t} \boldsymbol{\eta}_h^{m+1}) \right] \\ &\geq \frac{\delta t}{2} \frac{\gamma\mu}{h} \sum_{m=0}^{n-1} \left(\|\mathbf{u}_h^{m+1}\|_{0,\Sigma}^2 - \|\mathbf{u}_h^m\|_{0,\Sigma}^2 + \|\mathbf{u}_h^{m+1} - \mathbf{u}_h^m\|_{0,\Sigma}^2 \right. \\ &\quad \left. - \|\mathbf{u}_h^{m+1} - \mathbf{u}_h^m\|_{0,\Sigma}^2 - \|\mathbf{u}_h^{m+1} - \partial_{\delta t} \boldsymbol{\eta}_h^{m+1}\|_{0,\Sigma}^2 \right) \end{aligned}$$

Finally, using (23) we obtain

$$T_1 \geq \delta t \frac{\gamma \mu}{2h} \|\mathbf{u}_h^n\|_{0,\Sigma}^2 - \frac{C_\Sigma}{2} \|\mathbf{u}_h^0\|_{0,\Sigma}^2 - \delta t \frac{\gamma \mu}{4h} \sum_{m=0}^{n-1} \|\mathbf{u}_h^{m+1} - \partial_{\delta t} \boldsymbol{\eta}_h^{m+1}\|_{0,\Sigma}^2.$$

By inserting this expression in (25), its last term can be controlled thanks to the Nitsche dissipative term in E^n , which completes the proof. \square

The above Lemma shows that the first perturbation term in (22), involving the fluid velocity fluctuations at the interface, can be handled using the Nitsche penalty interface term in E^n , under the CFL-like condition (23). However, the second perturbation term in (22), involving the stress time fluctuations at the interface, can not be controlled by the discrete energy of the system E^n . Actually, the energy estimate fails to control the pressure fluctuations on the interface. Somehow this illustrates the infamous numerical instability featured by the explicit coupling scheme, when dealing with incompressible fluids.

We refer to [7] for a rigorous explanation of this issue in a simplified framework, relating the instability of the scheme to the fluid-solid density ratio ρ^f/ρ^s , irrespectively of the discretization parameters. A further analysis, considering different time discretization schemes, has been recently reported in [17]. In particular, the authors conclude that no sequentially staggered scheme can be constructed which would be unconditionally stable with respect to the fluid-solid density ratio.

Based on the above analysis, in the next section we propose a new explicit coupling scheme which, under condition (23), is unconditionally stable with respect to the fluid-solid density ratio.

5 Stabilized explicit coupling

In order to control the spurious oscillations of the fluid forces at the interface, arising in the energy estimate (24), we add to the fluid sub-problem (15) the following weakly consistent penalty term:

$$S_{\delta t}(\mathbf{U}_h^{n+1}, \mathbf{V}_h) \stackrel{\text{def}}{=} \gamma_0 \frac{\delta t}{\mu} \int_{\Sigma} \partial_{\delta t} \boldsymbol{\sigma}(\mathbf{u}_h^{n+1}, p_h^{n+1}) \mathbf{n} \cdot \boldsymbol{\sigma}(\mathbf{v}_h, q_h) \mathbf{n}, \quad (26)$$

with $\gamma_0 > 0$ to be chosen sufficiently large. Clearly, this corresponds to penalize the fluid force fluctuations on the fluid-structure interface Σ .

As a result, our new explicit coupling scheme is given by:

- **Solid sub-problem:** Given $(\mathbf{u}_h^n, p_h^n) \in W_h \times Q_h$, find $(\boldsymbol{\eta}_h^{n+1}, \dot{\boldsymbol{\eta}}_h^{n+1}) \in X_h \times X_h$ such that

$$\begin{aligned} A_{\delta t}^s((\boldsymbol{\eta}_h^{n+1}, \dot{\boldsymbol{\eta}}_h^{n+1}), (\mathbf{w}_h, \dot{\mathbf{w}}_h)) + \gamma \frac{\mu}{h} \int_{\Sigma} \partial_{\delta t} \boldsymbol{\eta}_h^{n+1} \cdot \mathbf{w}_h \\ = \gamma \frac{\mu}{h} \int_{\Sigma} \mathbf{u}_h^n \cdot \mathbf{w}_h - \int_{\Sigma} \boldsymbol{\sigma}(\mathbf{u}_h^n, p_h^n) \mathbf{n} \cdot \mathbf{w}_h, \end{aligned} \quad (27)$$

for all $(\mathbf{w}_h, \dot{\mathbf{w}}_h) \in X_h \times X_h$.

- **Fluid sub-problem:** Given $\partial_{\delta t} \boldsymbol{\eta}_h^{n+1} \in X_h$, find $(\mathbf{u}_h^{n+1}, p_h^{n+1}) \in W_h \times Q_h$, with $\mathbf{u}_h^{n+1} = \bar{\mathbf{u}}_h(t_{n+1})$ on Γ^{in} , such that

$$\begin{aligned} & A_{\delta t}^f((\mathbf{u}_h^{n+1}, p_h^{n+1}), (\mathbf{v}_h, q_h)) - \int_{\Sigma} \boldsymbol{\sigma}(\mathbf{u}_h^{n+1}, p_h^{n+1}) \mathbf{n} \cdot \mathbf{v}_h - \int_{\Sigma} \mathbf{u}_h^{n+1} \cdot \boldsymbol{\sigma}(\alpha \mathbf{v}_h, -q_h) \mathbf{n} \\ & + \gamma \frac{\mu}{h} \int_{\Sigma} \mathbf{u}_h^{n+1} \cdot \mathbf{v}_h + S_{\delta t}((\mathbf{u}_h^{n+1}, p_h^{n+1}), (\mathbf{v}_h, q_h)) = - \int_{\Sigma} \partial_{\delta t} \boldsymbol{\eta}_h^{n+1} \cdot \boldsymbol{\sigma}(\alpha \mathbf{v}_h, -q_h) \mathbf{n} \\ & \quad + \gamma \frac{\mu}{h} \int_{\Sigma} \partial_{\delta t} \boldsymbol{\eta}_h^{n+1} \cdot \mathbf{v}_h + \int_{\Gamma^{\text{out}}} \mathbf{g}(t_{n+1}) \cdot \mathbf{v}_h, \quad (28) \end{aligned}$$

for all $(\mathbf{v}_h, q_h) \in V_h \times Q_h$.

For the stability analysis below, we reformulate this new explicit coupling scheme in a monolithic fashion, by adding the expressions (27) and (28). This yields the problem: Find $(\mathbf{u}_h^{n+1}, p_h^{n+1}, \boldsymbol{\eta}_h^{n+1}, \dot{\boldsymbol{\eta}}_h^{n+1}) \in W_h \times Q_h \times X_h \times X_h$, with $\mathbf{u}_h^{n+1} = \bar{\mathbf{u}}_h(t_{n+1})$ on Γ^{in} , such that

$$\begin{aligned} & A_{\delta t}^f((\mathbf{u}_h, p_h), (\mathbf{v}_h, q_h)) + A_{\delta t}^s((\boldsymbol{\eta}_h, \dot{\boldsymbol{\eta}}_h), (\mathbf{w}_h, \dot{\mathbf{w}}_h)) \\ & - \int_{\Sigma} \boldsymbol{\sigma}(\mathbf{u}_h^{n+1}, p_h^{n+1}) \mathbf{n} \cdot \mathbf{v}_h + \int_{\Sigma} \boldsymbol{\sigma}(\mathbf{u}_h^n, p_h^n) \mathbf{n} \cdot \mathbf{w}_h \\ & - \int_{\Sigma} (\mathbf{u}_h^{n+1} - \partial_{\delta t} \boldsymbol{\eta}_h^{n+1}) \cdot \boldsymbol{\sigma}(\alpha \mathbf{v}_h, -q_h) \mathbf{n} + \gamma \frac{\mu}{h} \int_{\Sigma} (\mathbf{u}_h^{n+1} - \partial_t \boldsymbol{\eta}_h^{n+1}) \cdot \mathbf{v}_h \\ & - \gamma \frac{\mu}{h} \int_{\Sigma} (\mathbf{u}_h^n - \partial_t \boldsymbol{\eta}_h^{n+1}) \cdot \mathbf{w}_h + S_{\delta t}((\mathbf{u}_h^{n+1}, p_h^{n+1}), (\mathbf{v}_h, q_h)) \\ & = \int_{\Gamma^{\text{out}}} \mathbf{g}(t_{n+1}) \cdot \mathbf{v}_h, \end{aligned}$$

for all $(\mathbf{v}_h, q_h, \mathbf{w}_h, \dot{\mathbf{w}}_h) \in V_h \times Q_h \times X_h \times X_h$. Equivalently, in a more compact form,

$$A_S[(\mathbf{U}_h^{n+1}, \boldsymbol{\Theta}_h^{n+1}), (\mathbf{V}_h, \mathbf{W}_h)] = \int_{\Gamma^{\text{out}}} \mathbf{g}^{n+1} \cdot \mathbf{v}_h, \quad (29)$$

for all $(\mathbf{v}_h, q_h, \mathbf{w}_h, \dot{\mathbf{w}}_h) \in V_h \times Q_h \times X_h \times X_h$, where the stabilized explicit coupling bi-linear form A_S is given by

$$A_S[(\mathbf{U}_h^{n+1}, \boldsymbol{\Theta}_h^{n+1}), (\mathbf{V}_h, \mathbf{W}_h)] \stackrel{\text{def}}{=} A_E[(\mathbf{U}_h^{n+1}, \boldsymbol{\Theta}_h^{n+1}), (\mathbf{V}_h, \mathbf{W}_h)] + S_{\delta t}(\mathbf{U}_h^{n+1}, \mathbf{V}_h).$$

On the other hand, from (22), we obtain

$$\begin{aligned} A_S[(\mathbf{U}_h^{n+1}, \boldsymbol{\Theta}_h^{n+1}), (\mathbf{V}_h, \mathbf{W}_h)] & = A_I[(\mathbf{U}_h^{n+1}, \boldsymbol{\Theta}_h^{n+1}), (\mathbf{V}_h, \mathbf{W}_h)] \\ & \quad + \gamma \frac{\mu}{h} \int_{\Sigma} (\mathbf{u}_h^{n+1} - \mathbf{u}_h^n) \cdot \mathbf{w}_h \\ & \quad - \int_{\Sigma} (\boldsymbol{\sigma}(\mathbf{u}_h^{n+1}, p_h^{n+1}) \mathbf{n} - \boldsymbol{\sigma}(\mathbf{u}_h^n, p_h^n) \mathbf{n}) \cdot \mathbf{w}_h \\ & \quad + \gamma_0 \frac{\delta t}{\mu} \int_{\Sigma} \partial_{\delta t} \boldsymbol{\sigma}(\mathbf{u}_h^{n+1}, p_h^{n+1}) \mathbf{n} \cdot \boldsymbol{\sigma}(\mathbf{v}_h, q_h) \mathbf{n}. \end{aligned} \quad (30)$$

5.1 Stability analysis

In this section we will prove that the dissipative character of the Nitsche's penalty coupling term in combination with (26) makes the explicit scheme (14)-(15) stable, for γ_0 sufficiently large and under the CFL-like condition (23).

Theorem 5.1 *Assume that the fluid-structure system is isolated, i.e. $\bar{\mathbf{u}} = \mathbf{0}$ and $\mathbf{g} = \mathbf{0}$. Let $\{(\mathbf{u}_h^n, p_h^n, \boldsymbol{\eta}_h^n, \dot{\boldsymbol{\eta}}_h^n)\}_{0 \leq n \leq N-1}$ denote the solution of (27)-(28). Under the following conditions*

$$\begin{aligned} \gamma &> 8(1 + \alpha)C_{\text{TI}}, \\ \delta t &\leq \frac{C_\Sigma}{\gamma\mu} h, \\ \gamma_0 &> \left(\frac{4h}{\gamma} + 4C_{\text{KT}} \right), \end{aligned} \quad (31)$$

the following energy estimate holds, for $1 \leq n \leq N$,

$$\begin{aligned} E^n + 2\delta t \frac{\gamma\mu}{h} \|\mathbf{u}_h^n\|_{0,\Sigma}^2 + \frac{2\gamma_0\delta t}{\mu} \|\boldsymbol{\sigma}(\mathbf{u}_h^n, p_h^n)\mathbf{n}\|_{0,\Sigma}^2 \\ \leq 4E_0 + 2C_\Sigma \|\mathbf{u}_h^0\|_{0,\Sigma}^2 + \frac{2\gamma_0\delta t}{\mu} \|\boldsymbol{\sigma}(\mathbf{u}_h^0, p_h^0)\mathbf{n}\|_{0,\Sigma}^2. \end{aligned} \quad (32)$$

In other words, the stabilized explicit coupling scheme (27)-(28) is conditionally stable in the energy norm.

Proof. We proceed by first testing (29) with

$$(\mathbf{v}_h, q_h, \mathbf{w}_h, \dot{\mathbf{w}}_h) = (\mathbf{u}_h^{n+1}, p_h^{n+1}, \partial_{\delta t}\boldsymbol{\eta}_h^{n+1}, \partial_{\delta t}\dot{\boldsymbol{\eta}}_h^{n+1}).$$

Then, using (30), multiplying by δt , summing over $0 \leq m \leq n-1$ and using the stability analysis of the (unstabilized) explicit coupling scheme (Lemma 4.2), we obtain

$$\begin{aligned} E^n + \delta t \frac{\gamma\mu}{h} \|\mathbf{u}_h^n\|_{0,\Sigma}^2 + \underbrace{2 \frac{\gamma_0}{\mu} \delta t^2 \sum_{m=0}^{n-1} \int_{\Sigma} \partial_{\delta t}\boldsymbol{\sigma}(\mathbf{u}_h^{m+1}, p_h^{m+1})\mathbf{n} \cdot \boldsymbol{\sigma}(\mathbf{u}_h^{m+1}, p_h^{m+1})\mathbf{n}}_{T_1} \\ \leq 2E^0 + C_\Sigma \|\mathbf{u}_h^0\|_{0,\Sigma}^2 - \underbrace{2\delta t \sum_{m=0}^{n-1} \int_{\Sigma} (\boldsymbol{\sigma}(\mathbf{u}_h^{m+1}, p_h^{m+1})\mathbf{n} - \boldsymbol{\sigma}(\mathbf{u}_h^m, p_h^m)\mathbf{n}) \cdot \partial_{\delta t}\boldsymbol{\eta}_h^{m+1}}_{T_2}. \end{aligned} \quad (33)$$

In order to prove the stability of the scheme, we will show that the term $E^n + T_1$ can absorb the term T_2 .

First note that for the first term we have,

$$\begin{aligned} T_1 &= \frac{\gamma_0}{\mu} \delta t (\|\boldsymbol{\sigma}(\mathbf{u}_h^n, p_h^n)\mathbf{n}\|_{0,\Sigma}^2 - \|\boldsymbol{\sigma}(\mathbf{u}_h^0, p_h^0)\mathbf{n}\|_{0,\Sigma}^2) \\ &\quad + \frac{\gamma_0}{\mu} \delta t^3 \sum_{m=0}^{n-1} \|\partial_{\delta t}\boldsymbol{\sigma}(\mathbf{u}_h^{m+1}, p_h^{m+1})\mathbf{n}\|_{0,\Sigma}^2. \end{aligned} \quad (34)$$

Finally, term T_2 in (33), involving the fluid force fluctuations at the interface, can be bounded thanks to the new dissipative term T_1 . More precisely, we have

$$\begin{aligned}
T_2 &= -2\delta t^2 \sum_{m=0}^{n-1} \int_{\Sigma} \partial_{\delta t} \boldsymbol{\sigma}(\mathbf{u}_h^{m+1}, p_h^{m+1}) \mathbf{n} \cdot \partial_{\delta t} \boldsymbol{\eta}_h^{m+1} \\
&\leq 2\delta t^2 \sum_{m=0}^{n-1} \|\partial_{\delta t} \boldsymbol{\sigma}(\mathbf{u}_h^{m+1}, p_h^{m+1}) \mathbf{n}\|_{0,\Sigma} (\|\mathbf{u}_h^{m+1} - \partial_{\delta t} \boldsymbol{\eta}_h^{m+1}\|_{0,\Sigma} + \|\mathbf{u}_h^{m+1}\|_{0,\Sigma}) \\
&\leq \delta t^2 \sum_{m=0}^{n-1} \left[(\epsilon_1 + \epsilon_2) \frac{h}{\gamma \mu} \|\partial_{\delta t} \boldsymbol{\sigma}(\mathbf{u}_h^{m+1}, p_h^{m+1}) \mathbf{n}\|_{0,\Sigma}^2 \right. \\
&\quad \left. + \frac{1}{\epsilon_1} \frac{\gamma \mu}{h} \|\mathbf{u}_h^{m+1} - \partial_{\delta t} \boldsymbol{\eta}_h^{m+1}\|_{0,\Sigma}^2 + \frac{1}{\epsilon_2} \frac{\gamma \mu}{h} \|\mathbf{u}_h^{m+1}\|_{0,\Sigma}^2 \right] \\
&\leq \delta t^2 \sum_{m=0}^{n-1} \left[(\epsilon_1 + \epsilon_2) \frac{h}{\gamma \mu} \|\partial_{\delta t} \boldsymbol{\sigma}(\mathbf{u}_h^{m+1}, p_h^{m+1}) \mathbf{n}\|_{0,\Sigma}^2 \right. \\
&\quad \left. + \frac{1}{\epsilon_1} \frac{\gamma \mu}{h} \|\mathbf{u}_h^{m+1} - \partial_{\delta t} \boldsymbol{\eta}_h^{m+1}\|_{0,\Sigma}^2 + \frac{1}{\epsilon_2} \frac{\gamma \mu}{h} C_{\text{KT}} \|\boldsymbol{\epsilon}(\mathbf{u}_h^{m+1})\|_{0,\Omega^f}^2 \right],
\end{aligned}$$

where we have applied a trace inequality combined with the Poincaré's and Korn's inequalities. We now choose

$$\epsilon_1 = 4\delta t, \quad \epsilon_2 = \frac{4\gamma \delta t C_{\text{KT}}}{h},$$

to obtain

$$\begin{aligned}
T_2 &\leq \frac{\delta t^3}{\mu} \left(\frac{4h}{\gamma} + 4C_{\text{KT}} \right) \sum_{m=0}^{n-1} \|\partial_{\delta t} \boldsymbol{\sigma}(\mathbf{u}_h^{m+1}, p_h^{m+1}) \mathbf{n}\|_{0,\Sigma}^2 \\
&\quad + \delta t \sum_{m=0}^{n-1} \left(\frac{\gamma \mu}{4h} \|\mathbf{u}_h^{m+1} - \partial_{\delta t} \boldsymbol{\eta}_h^{m+1}\|_{0,\Sigma}^2 + \frac{\mu}{4} \|\boldsymbol{\epsilon}(\mathbf{u}_h^{m+1})\|_{0,\Omega^f}^2 \right).
\end{aligned} \tag{35}$$

By assuming that

$$\gamma_0 > \left(\frac{4h}{\gamma} + 4C_{\text{KT}} \right), \tag{36}$$

the first term, in the right hand side of (35), is absorbed by (34), using the dissipation of the stabilization term (26). The rest of terms are controlled, as usual, by the dissipative penalty Nitsche coupling and the viscous dissipation of the fluid in E^n . We obtain the desired estimate by inserting the bounds (34) and (35) in (33), which completes the proof. \square

We conclude this section with a series of remarks.

Remark 5.2 *According to Theorem 5.1, the stability of the scheme is independent of the fluid-solid density ratio ρ^f/ρ^s . This is a major advantage compared to the standard explicit-coupling, whose (in)stability precisely relies on this ratio, irrespectively of the discretization parameters (see [7, 17]).*

Remark 5.3 *The proof of Theorem 5.1 is based, exclusively, on the dissipation due to the Nitsche coupling and the time force penalization terms. As a result,*

our stability result is independent of the dissipative features of the fluid and solid time discretization schemes. This is a significant progress with respect to the stability result stated in [13], for a semi-implicit coupling scheme, whose proof purely depends on the dissipative properties of the solid time discretization scheme (a leap-frog scheme). On the other hand, as regards the fluid time-discretization, one can use, for instance, a neutrally stable second order scheme.

Remark 5.4 *Because of their common structure, we have used the terminology CFL for the stability condition $(31)_2$. However, we must stress that their nature and impact on the numerical solution are completely different. Actually, from the proof of Lemma 4.2, one can notice that $(31)_2$ does not arise from bounding amplification factors, which is indeed the case for the classical CFL condition. As a result, failing to satisfy $(31)_2$ only indicates that the constant C_Σ is not h -uniform. In particular, according to the energy estimate (32), for $h > 0$ (fixed) the numerical solution remains always bounded, irrespectively of n , so no CFL time blow-up appears.*

5.2 Stabilization and artificial compressibility

In this paragraph we motivate the role of the time-penalty term (26) as a quasi-incompressible approximation at the discrete level. For the sake of clarity, we neglect the viscous term in (26) so that the stabilization term reduces to

$$S_{\delta t}(p_h^{n+1}, q_h) \stackrel{\text{def}}{=} \gamma_0 \frac{\delta t}{\mu} \int_{\Sigma} \partial_{\delta t} p_h^{n+1} q_h.$$

As a result, the discrete continuity equation in (28) is given by

$$\gamma_0 \frac{\delta t}{\mu} \int_{\Sigma} \partial_{\delta t} p_h^{n+1} q_h + \int_{\Omega^f} q_h \nabla \cdot \mathbf{u}_h^{n+1} = 0,$$

for all $q_h \in Q_h$, which corresponds to the discrete counterpart of the modified continuity equation

$$c_{\delta t, \Sigma} \partial_t p + \nabla \cdot \mathbf{u} = 0, \quad \text{in } \Omega^f.$$

Here, $c_{\delta t, \Sigma} \stackrel{\text{def}}{=} (\gamma_0 \delta t / \mu) \delta_\Sigma$ can be thought as an artificial compressibility parameter, where δ_Σ stands for the Dirac measure on the surface Σ .

We can, therefore, interpret the stabilization of the explicit coupling scheme (26) as a quasi-incompressible approximation. Let us note that, the artificial compressibility $c_{\delta t, \Sigma}$ is purely restricted to the wall Σ , through the Dirac measure δ_Σ . In practice, it is limited to the first layer of fluid mesh elements from the interface Σ . Formally, $c_{\delta t, \Sigma}$ goes to zero as long as $\delta t \rightarrow 0$. Actually, we shall see in the next paragraph that, under suitable assumptions on the discretization parameters, the penalty term (26) is of order $O(\delta t^{\frac{1}{2}})$, and hence consistent with the original equation.

The role of the divergence-free constraint in the fluid-structure coupling has already been outlined in the literature. Let us cite, for instance, the work [36, 23], where quasi-compressibility is introduced in order to accelerate the convergence of fixed-point iterations towards the solution of an implicit coupling scheme. Here, the quasi-compressibility vanishes at convergence and the artificial compressibility parameter is chosen so as to optimize efficiency (it only depends on physical quantities) and not for consistency or stability purposes.

Finally, let us mention the non-consistent approach where artificial compressibility could be introduced at the continuous level [11], in order to avoid explicit coupling instabilities.

5.3 Weak consistency and error estimates

The stability estimate obtained in §5.1 may now be used to derive formal a priori error estimates. The structure is discretized in time using a conservative and second order Newmark's scheme. The fluid, on the other hand, is expected to be first order in time due to the backward Euler discretization. This is indeed the order of the fully implicit scheme on a fixed mesh. In the explicit scheme, however, the penalization of the interface force time fluctuations, on the fluid side, is only weakly consistent. We will now show that this weak consistency causes a loss of half a power in δt , *i.e.* that we may expect only $O(\delta t^{\frac{1}{2}})$ convergence in time. On the other hand, we will see that the Nitsche's penalty term introduces a non-trivial interaction between the time and space discretization, specially in the case of the explicit coupling. In practice, this results in a h -non-uniformity of the constant involved in the time truncation error, which requires a balancing of the space and time discretization parameters in order to retain optimal convergence asymptotically.

Let the hypothesis of Theorem 5.1 be satisfied, moreover assume that there exists an optimal order interpolation operator π_h that enjoys the following additional stability property:

$$\|\boldsymbol{\sigma}(\pi_h \mathbf{u}, \pi_h p)\|_{0,\Sigma} + \|\pi_h \mathbf{u}\|_{0,\Sigma} \leq C,$$

where $C > 0$ is a constant independent of h . This can be expected to hold true for sufficiently regular solutions (\mathbf{u}, p) . In particular, it can be shown to hold in the case when $(\mathbf{u}, p) \in [W^{1,\infty}(\Omega^f)]^d \times H^1(\Omega^f)$.

We do not make a full convergence analysis in this paper, but we will simply detail the terms that enter in the (formal) upper bound of the error and show that the order is $O(\delta t^{\frac{1}{2}})$ for fixed h .

Let $\boldsymbol{\theta}_h^m \stackrel{\text{def}}{=} \mathbf{u}_h^m - \pi_h \mathbf{u}(t_m)$, $y_h^m \stackrel{\text{def}}{=} p_h^m - \pi_h p(t_m)$, $\boldsymbol{\xi}_h^m \stackrel{\text{def}}{=} \boldsymbol{\eta}_h^m - \pi_h \boldsymbol{\eta}(t_m)$ and $\dot{\boldsymbol{\xi}}_h^m \stackrel{\text{def}}{=} \dot{\boldsymbol{\eta}}_h^m - \pi_h \dot{\boldsymbol{\eta}}(t_m)$ be the discrete errors. We introduce the following discrete error functional

$$\begin{aligned} \mathcal{E}^n &= \frac{\rho^f}{2} \|\boldsymbol{\theta}_h^n\|_{0,\Omega^f}^2 + \frac{\rho^s}{2} \|\dot{\boldsymbol{\xi}}_h^n\|_{0,\Omega^s}^2 + \frac{1}{2} a^s(\boldsymbol{\xi}_h^n, \boldsymbol{\xi}_h^n) + \delta t \frac{\mu}{2} \sum_{m=0}^{n-1} \|\boldsymbol{\epsilon}(\boldsymbol{\theta}_h^{m+1})\|_{0,\Omega^f}^2 \\ &\quad + \frac{\gamma_0 \delta t}{\mu} \|\boldsymbol{\sigma}(\boldsymbol{\theta}_h^n, y_h^n)\|_{0,\Sigma}^2 + \delta t \frac{\gamma \mu}{2h} \sum_{m=0}^{n-1} \|\boldsymbol{\theta}_h^{m+1} - \partial_{\delta t} \boldsymbol{\xi}_h^{m+1}\|_{0,\Sigma}^2. \end{aligned}$$

A formal error estimate for our formulation can be obtained using the stability result of Theorem 5.1, on the discrete error quantities $\boldsymbol{\xi}_h^n$, $\boldsymbol{\theta}_h^n$, and y_h^n , followed by an application of the (modified) Galerkin orthogonality, which gives rise to the following upper bound of the error:

$$\mathcal{E}^n \leq C \left(\tau(\delta t, h)^2 + \sum_{j=1}^4 \tau_j \right), \quad (37)$$

and $C > 0$ is a generic constant independent of h , δt , n and T . The term $\tau(\delta t, h)$ is a truncation error of optimal order, that comes from the finite difference time discretization and the space finite element approximation in each subdomain. The remaining consistency terms are given by:

$$\begin{aligned}
\tau_1 &\stackrel{\text{def}}{=} \frac{\gamma\mu}{h} \delta t \sum_{m=0}^{n-1} \int_{\Sigma} (\partial_t \boldsymbol{\eta}(t_{m+1}) - \partial_{\delta t} \boldsymbol{\eta}(t_{m+1})) \cdot (\boldsymbol{\theta}_h^{m+1} - \partial_{\delta t} \boldsymbol{\xi}_h^{m+1}), \\
\tau_2 &\stackrel{\text{def}}{=} \delta t^2 \sum_{m=0}^{n-1} \int_{\Sigma} \partial_{\delta t} \boldsymbol{\sigma}(\pi_h \mathbf{u}(t_{m+1}), \pi_h p(t_{m+1})) \mathbf{n} \cdot \boldsymbol{\theta}_h^{m+1}, \\
\tau_3 &\stackrel{\text{def}}{=} \frac{\gamma\mu}{h} \delta t^2 \sum_{m=0}^{n-1} \int_{\Sigma} \partial_{\delta t} \pi_h \mathbf{u}(t_{m+1}) \cdot \partial_{\delta t} \boldsymbol{\xi}_h^{m+1}, \\
\tau_4 &\stackrel{\text{def}}{=} \frac{\gamma_0}{\mu} \delta t^2 \sum_{m=0}^{n-1} \int_{\Sigma} \partial_{\delta t} \boldsymbol{\sigma}(\pi_h \mathbf{u}(t_{m+1}), \pi_h p(t_{m+1})) \mathbf{n} \cdot \boldsymbol{\sigma}(\boldsymbol{\theta}_h^{m+1}, \mathbf{y}_h^{m+1}) \mathbf{n}.
\end{aligned} \tag{38}$$

The first term, τ_1 , arises from the first order time discretization of the interface coupling condition, $\mathbf{u} = \partial_t \boldsymbol{\eta}$ on Σ , in (28). Note that this term also appears in the consistency analysis of the implicit coupling scheme (14)-(15). Terms τ_2 and τ_3 come from the explicit treatment of the interface coupling conditions and, finally, τ_4 results from the time penalty stabilization term (26).

We will here only derive the upper bounds for τ_1 , τ_3 and τ_4 , since all the difficulties are encountered in these terms and they give the final order.

For the first term we use the standard truncation error estimate

$$|\partial_t \boldsymbol{\eta}(t_{m+1}) - \partial_{\delta t} \boldsymbol{\eta}(t_{m+1})| \leq \int_{t^m}^{t_{m+1}} |\partial_{tt} \boldsymbol{\eta}| \leq \delta t^{\frac{1}{2}} \left(\int_{t^m}^{t_{m+1}} |\partial_{tt} \boldsymbol{\eta}|^2 \right)^{\frac{1}{2}}.$$

Thus, we have

$$\begin{aligned}
\tau_1 &\leq \frac{\gamma\mu}{h} \delta t^{\frac{3}{2}} \sum_{m=0}^{n-1} \|\partial_{tt} \boldsymbol{\eta}\|_{0, \Sigma \times (t_m, t_{m+1})} \|\boldsymbol{\theta}_h^{m+1} - \partial_{\delta t} \boldsymbol{\xi}_h^{m+1}\|_{0, \Sigma} \\
&\leq \frac{1}{2\epsilon} \frac{\gamma\mu \delta t^2}{h} \|\partial_{tt} \boldsymbol{\eta}\|_{0, \Sigma \times (0, T)}^2 + \frac{\epsilon}{2} \frac{\gamma\mu}{h} \delta t \sum_{m=0}^{n-1} \|\boldsymbol{\theta}_h^{m+1} - \partial_{\delta t} \boldsymbol{\xi}_h^{m+1}\|_{0, \Sigma}^2,
\end{aligned} \tag{39}$$

with $\epsilon > 0$ to be chosen below.

The third term is treated as follows

$$\begin{aligned}
\tau_3 &= \frac{\gamma\mu}{h} \delta t^2 \sum_{m=0}^{n-1} \int_{\Sigma} \partial_{\delta t} \pi_h \mathbf{u}(t_{m+1}) \cdot (\partial_{\delta t} \boldsymbol{\xi}_h^{m+1} - \boldsymbol{\theta}_h^{m+1} + \boldsymbol{\theta}_h^{m+1}) \\
&= \underbrace{\frac{\gamma\mu}{h} \delta t^2 \sum_{m=0}^{n-1} \int_{\Sigma} \partial_{\delta t} \pi_h \mathbf{u}(t_{m+1}) \cdot (\partial_{\delta t} \boldsymbol{\xi}_h^{m+1} - \boldsymbol{\theta}_h^{m+1})}_{T_1} \\
&\quad + \underbrace{\frac{\gamma\mu}{h} \delta t^2 \sum_{m=0}^{n-1} \int_{\Sigma} \partial_{\delta t} \pi_h \mathbf{u}(t_{m+1}) \cdot \boldsymbol{\theta}_h^{m+1}}_{T_2}.
\end{aligned}$$

For the finite difference $\partial_{\delta t}\pi_h\mathbf{u}(t_{m+1})$ we use the truncation error estimate

$$|\partial_{\delta t}\pi_h\mathbf{u}(t_{m+1})| = \frac{1}{\delta t} \int_{t^m}^{t^{m+1}} |\partial_t\pi_h\mathbf{u}| \leq \frac{1}{\delta t^{\frac{1}{2}}} \left(\int_{t^m}^{t^{m+1}} |\partial_t\pi_h\mathbf{u}|^2 \right)^{\frac{1}{2}}. \quad (40)$$

Hence, the term T_1 is upper bounded by

$$\begin{aligned} T_1 &\leq \frac{\gamma\mu}{h} \delta t^{\frac{3}{2}} \sum_{m=0}^{n-1} \|\partial_t\pi_h\mathbf{u}\|_{0,\Sigma \times (t_m, t_{m+1})} \|\boldsymbol{\theta}_h^{m+1} - \partial_{\delta t}\boldsymbol{\xi}_h^{m+1}\|_{0,\Sigma} \\ &\leq \frac{1}{2\epsilon} \frac{\gamma\mu\delta t^2}{h} \|\partial_t\pi_h\mathbf{u}\|_{0,\Sigma \times (0,T)}^2 + \frac{\epsilon}{2} \frac{\gamma\mu}{h} \delta t \sum_{m=0}^{n-1} \|\boldsymbol{\theta}_h^{m+1} - \partial_{\delta t}\boldsymbol{\xi}_h^{m+1}\|_{0,\Sigma}^2. \end{aligned} \quad (41)$$

In a similar fashion, using now the trace inequality combined with Poincaré's and Korn's inequalities, $\|\boldsymbol{\theta}_h^m\|_{0,\Sigma} \leq C_{\text{KT}}\|\boldsymbol{\epsilon}(\boldsymbol{\theta}_h^m)\|_{0,\Omega^f}$, we obtain the following bound for T_2 :

$$T_2 \leq \frac{1}{2\epsilon} \frac{\gamma^2 C_{\text{KT}}^2 \mu \delta t^2}{h^2} \|\partial_t\pi_h\mathbf{u}\|_{0,\Sigma \times (0,T)}^2 + \frac{\epsilon}{2} \mu \delta t \sum_{m=0}^{n-1} \|\boldsymbol{\epsilon}(\boldsymbol{\theta}_h^m)\|_{0,\Omega^f}^2. \quad (42)$$

Finally, by applying the estimate (40) to $|\partial_{\delta t}\boldsymbol{\sigma}(\pi_h\mathbf{u}(t_{m+1}), \pi_h p(t_{m+1}))\mathbf{n}|$, from (38) it follows that

$$\begin{aligned} \tau_4 &\leq \frac{\gamma_0 T}{2\mu} \delta t \|\partial_t\boldsymbol{\sigma}(\pi_h\mathbf{u}, \pi_h p)\mathbf{n}\|_{0,\Sigma \times (0,T)}^2 \\ &\quad + \frac{\gamma_0}{2\mu} \frac{\delta t^2}{T} \sum_{m=0}^{n-1} \|\boldsymbol{\sigma}(\boldsymbol{\theta}_h^{m+1}, y_h^{m+1})\mathbf{n}\|_{0,\Sigma}^2. \end{aligned} \quad (43)$$

We now take $\epsilon = (3C)^{-1}$ and insert the estimates (39)-(43) in (37) to obtain

$$\begin{aligned} \mathcal{E}^n &\leq C \left\{ 2\tau(\delta t, h)^2 + \frac{\gamma_0}{\mu} \frac{\delta t^2}{T} \sum_{m=0}^{n-1} \|\boldsymbol{\sigma}(\boldsymbol{\theta}_h^{m+1}, y_h^{m+1})\mathbf{n}\|_{0,\Sigma}^2 \right. \\ &\quad + 3C \left[\frac{\gamma\mu\delta t^2}{h} \left(\|\partial_{tt}\boldsymbol{\eta}\|_{0,\Sigma \times (0,T)}^2 + \|\partial_t\pi_h\mathbf{u}\|_{0,\Sigma \times (0,T)}^2 \right) \right. \\ &\quad \left. \left. + \frac{\gamma^2 C_{\text{KT}}^2 \mu \delta t^2}{h^2} \|\partial_t\pi_h\mathbf{u}\|_{0,\Sigma \times (0,T)}^2 \right] \right. \\ &\quad \left. + \frac{\gamma_0 T}{\mu} \delta t \|\partial_t\boldsymbol{\sigma}(\pi_h\mathbf{u}, \pi_h p)\mathbf{n}\|_{0,\Sigma \times (0,T)}^2 \right\}. \end{aligned}$$

Therefore, by applying Gronwall's Lemma and using the stability of the projection π_h , we have

$$\mathcal{E}^n \leq C \left(\tau(\delta t, h)^2 + \frac{\gamma\mu\delta t^2}{h} + \frac{\gamma^2 C_{\text{KT}}^2 \mu \delta t^2}{h^2} + \frac{\gamma_0 T}{\mu} \delta t \right). \quad (44)$$

Several remarks are in order. First of all the estimate (44) shows that, on a fixed mesh, the convergence order in time is imposed by the inconsistency of the time penalization (26), namely, the last term in (44) which scales as $O(\delta t^{\frac{1}{2}})$.

This is a typical reduction of order for splitting schemes, observed for instance in velocity-pressure splitting schemes of Chorin-Temam type for the Navier-Stokes equations. The other two terms are of order δt on a fixed mesh. However, in this case, the constant depends on h and we see that asymptotically, *i.e.* when refining both in h and in δt , we will have to chose $\delta t = O(h^2)$ in order to keep uniformity. Such a choice leads to the estimate

$$\mathcal{E}^n \leq C(\tau(\delta t, h)^2 + Th^2),$$

which is optimal in the energy norm if piecewise linear finite elements are used for the discretization of the fluid velocities and the structure displacements.

Remark 5.5 *Note that in the case of the implicit coupling scheme, estimate (44) reduces to*

$$\mathcal{E}^n \leq C\left(\tau(\delta t, h)^2 + \frac{\gamma\mu\delta t^2}{h}\right).$$

We therefore recover an optimal $O(\delta t)$ on a fixed mesh. As for the explicit coupling, the constant appearing in the error estimate still depends on h , due to the Nitsche penalty term. However, here, it is sufficient to take $\delta t = O(h^{\frac{3}{2}})$ in order to keep optimality asymptotically.

5.4 Improving time accuracy: defect-correction iterations

In this paragraph we propose to recover optimal accuracy in time, namely $O(\delta t)$, by performing a few iterations based on the defect-correction method.

The *iterative defect-correction* method (see *e.g.* [37]) is an iterative procedure which aims at increasing the accuracy of a numerical solution, without mesh refinement. The basic principle of the method is based on the “neighboring problem” idea, which can be described as follows (we refer to [37] for the details). Assume that we want to approximate the solution x^* of the equation

$$F(x) = 0, \tag{45}$$

by solving a related problem

$$\tilde{F}(x) = 0, \tag{46}$$

whose solution operator is denoted by \tilde{G} , *i.e.* $\tilde{F}(\tilde{G}(0)) = 0$. Let $x_0 = \tilde{G}(0)$ be the approximation of x^* obtained by solving problem (46). The key point now is to estimate the error $x^* - x_0$. First, note that x_0 is solution of the problem

$$F(x) = F(x_0), \tag{47}$$

which is a “neighboring problem” of (45). The “neighboring problem” idea consists in assuming that the error generated by the solution operator \tilde{G} is nearly the same for both problems, (45) and (47), *i.e.*

$$x^* - x_0 \approx x_0 - \tilde{G}(F(x_0)),$$

or

$$x^* \approx x_0 + \left[x_0 - \tilde{G}(F(x_0)) \right].$$

This last expression motivates an improved approximation of x^* , x_1 , by setting

$$x_1 = x_0 + (x_0 - \tilde{G}(F(x_0))).$$

The procedure can be repeated iteratively, which leads to the so-called defect-correction method

$$x_{k+1} = x_0 + \left[x_k - \tilde{G}(F(x_k)) \right] = x_0 + \left(\tilde{G} \circ \tilde{F} - \tilde{G} \circ F \right) (x_k),$$

for $k \geq 0$. If \tilde{G} is an affine mapping, the above iterations reduce to

$$x_{k+1} = \tilde{G}(\tilde{F}(x_k) - F(x_k)),$$

for $k \geq 0$, or equivalently

$$\tilde{F}(x_{k+1}) = \tilde{F}(x_k) - F(x_k), \quad k \geq 0, \quad (48)$$

which defines an alternative version of the defect-correction method.

We now propose to make use of this iterations in order to improve the accuracy of the stabilized explicit scheme (27)-(28). More precisely, we want to recover the accuracy of the implicit scheme (18) with a few iterations of (48) per time step, involving the stabilized explicit scheme.

In terms of the above notations we then set:

$$\begin{aligned} x &\stackrel{\text{def}}{=} (\mathbf{U}_h^{n+1}, \boldsymbol{\Theta}_h^{n+1}), \\ \langle F(x), (\mathbf{V}_h, \mathbf{W}_h) \rangle &\stackrel{\text{def}}{=} A_I[(\mathbf{U}_h^{n+1}, \boldsymbol{\Theta}_h^{n+1}), (\mathbf{V}_h, \mathbf{W}_h)] - \int_{\Gamma^{\text{out}}} \mathbf{g}(t_{n+1}) \cdot \mathbf{v}_h, \\ \langle \tilde{F}(x), (\mathbf{V}_h, \mathbf{W}_h) \rangle &\stackrel{\text{def}}{=} A_S[(\mathbf{U}_h^{n+1}, \boldsymbol{\Theta}_h^{n+1}), (\mathbf{V}_h, \mathbf{W}_h)] - \int_{\Gamma^{\text{out}}} \mathbf{g}(t_{n+1}) \cdot \mathbf{v}_h. \end{aligned}$$

Thus, from (30), the *defect difference* $\langle \tilde{F}(x_k) - F(x_k), (\mathbf{V}_h, \mathbf{W}_h) \rangle$ is given by

$$\begin{aligned} &\gamma_0 \frac{\delta t}{\mu} \int_{\Sigma} \frac{1}{\delta t} \left(\boldsymbol{\sigma}(\mathbf{u}_h^{n+1,k}, p_h^{n+1,k}) \mathbf{n} - \boldsymbol{\sigma}(\mathbf{u}_h^n, p_h^n) \mathbf{n} \right) \cdot \boldsymbol{\sigma}(\mathbf{v}_h, q_h) \mathbf{n} \\ &+ \gamma \frac{\mu}{h} \int_{\Sigma} \left(\mathbf{u}_h^{n+1,k} - \mathbf{u}_h^n \right) \cdot \dot{\mathbf{w}}_h - \int_{\Sigma} \left(\boldsymbol{\sigma}(\mathbf{u}_h^{n+1,k}, p_h^{n+1,k}) \mathbf{n} - \boldsymbol{\sigma}(\mathbf{u}_h^n, p_h^n) \mathbf{n} \right) \cdot \dot{\mathbf{w}}_h. \end{aligned}$$

As a result, the stabilized explicit scheme (27)-(28) combined with $K \geq 1$ defect-correction iterations, (48), leads to the following iterative procedure:

- **Time loop:** For $0 \leq n \leq N - 1$ let

$$(\mathbf{u}_h^{n+1,0}, p_h^{n+1,0}) \stackrel{\text{def}}{=} (\mathbf{u}_h^n, p_h^n)$$

- **Correction loop:** For $0 \leq k \leq K$, solve:

1. **Solid substep:** Find $(\boldsymbol{\eta}_h^{n+1,k+1}, \dot{\boldsymbol{\eta}}_h^{n+1,k+1}) \in X_h \times X_h$ such that

$$\begin{aligned} &A_{\delta t}^S((\boldsymbol{\eta}_h^{n+1,k+1}, \dot{\boldsymbol{\eta}}_h^{n+1,k+1}), (\mathbf{w}_h, \dot{\mathbf{w}}_h)) + \gamma \frac{\mu}{h} \int_{\Sigma} \partial_{\delta t} \boldsymbol{\eta}_h^{n+1,k+1} \cdot \mathbf{w}_h \\ &= \gamma \frac{\mu}{h} \int_{\Sigma} \mathbf{u}_h^{n+1,k} \cdot \mathbf{w}_h - \int_{\Sigma} \boldsymbol{\sigma}(\mathbf{u}_h^{n+1,k}, p_h^{n+1,k}) \mathbf{n} \cdot \mathbf{w}_h, \quad (49) \end{aligned}$$

for all $(\dot{\mathbf{w}}_h, \mathbf{w}_h) \in X_h \times X_h$.

2. **Fluid substep:** Find $(\mathbf{u}_h^{n+1,k+1}, p_h^{n+1,k+1}) \in W_h \times Q_h$ with $\mathbf{u}_h^{n+1,k+1} = \bar{\mathbf{u}}_h(t_{n+1})$ on Γ^{in} , such that

$$\begin{aligned}
& A_{\delta t}^f((\mathbf{u}_h^{n+1,k+1}, p_h^{n+1,k+1}), (\mathbf{v}_h, q_h)) - \int_{\Sigma} \boldsymbol{\sigma}(\mathbf{u}_h^{n+1,k+1}, p_h^{n+1,k+1}) \mathbf{n} \cdot \mathbf{v}_h \\
& - \int_{\Sigma} \mathbf{u}_h^{n+1,k+1} \cdot \boldsymbol{\sigma}(\alpha \mathbf{v}_h, -q_h) \mathbf{n} + \gamma \frac{\mu}{h} \int_{\Sigma} \mathbf{u}_h^{n+1,k+1} \cdot \mathbf{v}_h \\
& + \frac{\gamma_0}{\mu} \int_{\Sigma} \left(\boldsymbol{\sigma}(\mathbf{u}_h^{n+1,k+1}, p_h^{n+1,k+1}) - \boldsymbol{\sigma}(\mathbf{u}_h^{n+1,k}, p_h^{n+1,k}) \right) \cdot \boldsymbol{\sigma}(\mathbf{v}_h, q_h) \mathbf{n} \\
& = - \int_{\Sigma} \partial_{\delta t} \boldsymbol{\eta}_h^{n+1,k+1} \cdot \boldsymbol{\sigma}(\alpha \mathbf{v}_h, -q_h) \mathbf{n} + \gamma \frac{\mu}{h} \int_{\Sigma} \partial_{\delta t} \boldsymbol{\eta}_h^{n+1,k+1} \cdot \mathbf{v}_h \\
& \quad + \int_{\Gamma^{\text{out}}} \mathbf{g}(t_{n+1}) \cdot \mathbf{v}_h, \quad (50)
\end{aligned}$$

for all $(\mathbf{v}_h, q_h) \in V_h \times Q_h$.

Here, we used the notation $\partial_{\delta t} X^{n+1,q} \stackrel{\text{def}}{=} (X^{n+1,q} - X^n) / \delta t$.

Remark 5.6 Note that, for $K = 0$ (i.e. with no corrections) the above algorithm reduces to the original stabilized explicit coupling scheme (27)-(28).

One of the main features of the above algorithm is that the corrected solution at step $k \geq 0$ is expected to be of order $O(\delta t + (\delta t)^{\frac{k+1}{2}})$. So, one defect-correction iteration is enough to recover first order optimality. This will be illustrated with numerical results in the next section. The corresponding theoretical convergence analysis of (49)-(50) is beyond the scope of this paper. The interested reader is referred to [24] where error estimates of defect-corrections methods are obtained in a different framework.

6 Numerical experiments

In this section we illustrate the properties of the stabilized explicit coupling scheme (49)-(50), with $K \geq 0$ corrections, by performing a series of numerical experiments.

6.1 A two-dimensional test case

We consider a simplified version of the numerical experiment reported in [31, 16], by coupling the 2D Stokes equations with the linear elasticity equations. The

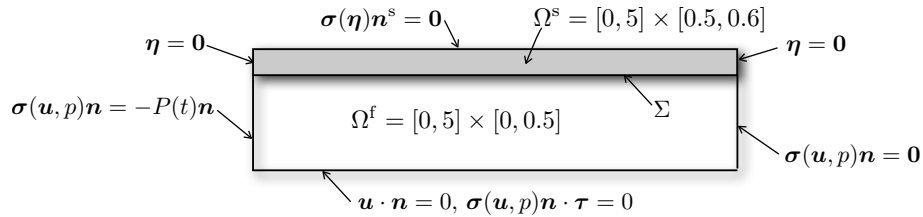


Figure 2: Geometrical description and boundary conditions

fluid domain is given by $\Omega^f \stackrel{\text{def}}{=} [0, 5] \times [0, 0.5]$ and the solid domain by $\Omega^s \stackrel{\text{def}}{=} [0, 5] \times [0.5, 0.6]$, all the space units are in cm.

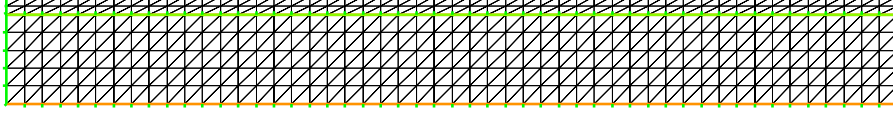


Figure 3: Fluid and solid finite element meshes

Both systems, the fluid and the structure, are initially at rest. We impose, between $x = 0$ and $x = 5$, an over pressure of $P = 10^4$ dyne/cm² during 5×10^{-3} s. The structure is clamped on $x = 0$ and $x = 5$ and zero traction is applied on $y = 0.6$ (see Figure 2). The fluid physical parameters are given by $\rho^f = 1.1$ g/cm³ and $\mu = 0.035$ poise. For the solid we have $\rho^s = 1.2$ g/cm³, $E = 3 \times 10^8$ dyne/cm² for the Young modulus and a Poisson ratio of $\nu = 0.3$.

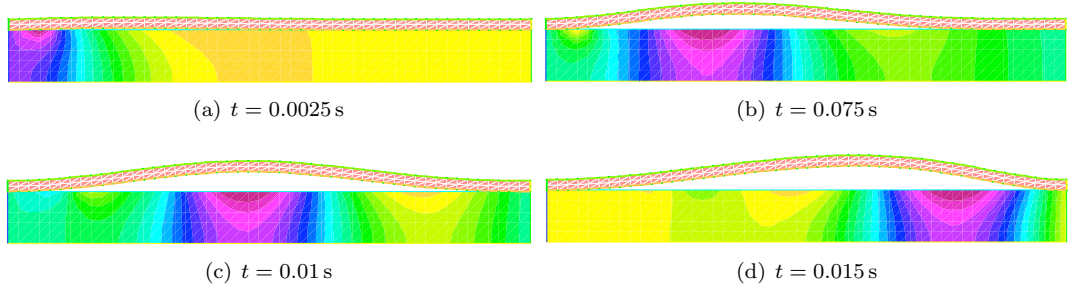


Figure 4: Stabilized explicit coupling ($K = 0$, $\alpha = 1$, $\gamma = 100$, $\gamma_0 = 8.75 \times 10^{-4}$): snapshots of the pressure and solid deformation (exaggerated) at four time instants.

For the discretization in space we used the Taylor-Hood finite element for the fluid equations and a standard \mathbb{P}_1 -continuous discretization for the structure. The mesh size was set to $h = 0.1$ (see Figure 3). Except when specifically mentioned, we consider the symmetric formulation ($\alpha = 1$). The time step is fixed to $\delta t = 10^{-4}$ s, the Nitsche penalty to $\gamma = 100$ and the time penalty parameter to $\gamma_0 = 8.75 \times 10^{-4}$, in the case without correction ($K = 0$), and to $\gamma_0 = 3.5 \times 10^{-5}$ with correction ($K \geq 1$). The numerical computations have been performed with FreeFem++ [22].

Let us consider, first, the stabilized explicit coupling scheme (49)-(50) without correction, *i.e.* $K = 0$, (equivalent to (27)-(28)). In Figure 4 we have reported the computed pressure contours and the solid deformed configuration at four time instants. The interface mid-point y -displacement and the out-flow are depicted in Figure 5. As predicted by Theorem 5.1 the numerical solution is stable, and we can observe a pressure wave that propagates through the fluid domain (see *e.g* [31, 9]).

We now investigate the impact of the fluid-solid density ratio ρ^f/ρ^s on the stability of the stabilized explicit coupling. To this aim, we keep constant the solid density, $\rho^s = 1.2$, and we take ρ^f ranging from 10^{-2} to 10^3 . The corresponding interface mid-point vertical displacements are shown in Figure 6.

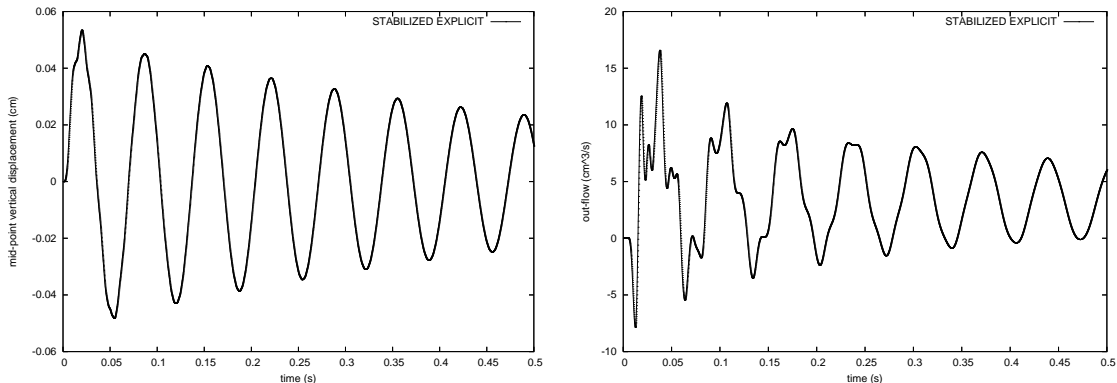


Figure 5: Stabilized explicit coupling ($K = 0$, $\alpha = 1$, $\gamma = 100$, $\gamma_0 = 8.75 \times 10^{-4}$): interface mid-point y -displacement and out-flow

We can notice that, according to Theorem 5.1 and Remark 5.2, the numerical solution remains stable irrespectively of the fluid-solid density ratio.

Let us turn our attention to the accuracy of the numerical solution provided by the stabilized explicit coupling scheme without correction ($K = 0$). In Figure 7, we make a comparison of the interface mid-point vertical displacement and the out-flow obtained with the stabilized explicit coupling and the implicit coupling, (14)-(15) with $\mathbf{u}_h^* = \mathbf{u}_h^{n+1}$, $p_h^* = p_h^{n+1}$, $\alpha = 1$ and $\gamma = 100$. The latter being solved by relaxed sub-iterations between (14) and (15) (see *e.g.* [28]). The poor accuracy of the numerical solution provided by the stabilized explicit coupling scheme (without correction) is clearly visible, both amplitude and phase are unsatisfactory. This sub-optimality is in agreement with the formal consistency analysis performed in Paragraph §5.3. Indeed, for the stabilized explicit coupling scheme (27)-(28) the convergence rate (in time) is expected to be $O(\delta t^{\frac{1}{2}})$, whereas for the implicit scheme an optimal $O(\delta t)$ is predicted. Figure 8 shows that, for a sufficiently small time step, the stabilized explicit coupling solution reaches the accuracy of the implicit coupling scheme. Clearly, improving the accuracy of the stabilized explicit solution by reducing the time step is inefficient in practice.

We shall see below that, according to Paragraph §5.4, one defect-correction iteration ($K = 1$) is enough to recover optimal accuracy. In the meantime, we propose to illustrate, with a series of numerical computations, the relevance of the stability condition (31) and the error estimate (44).

Let us consider a fixed time step $\delta t = 10^{-4}$ s and take as reference solution the one provided by the implicit coupling scheme ($\gamma = 100$, $\alpha = 1$). We then compute the relative out-flow l^2 -errors obtained with the stabilized explicit coupling scheme ($K = 0$), for different values of γ and γ_0 . The corresponding relative errors are given in Table 1, for the symmetric formulation ($\alpha = 1$), and in Table 2, for the non-symmetric ($\alpha = -1$). The symbol “X” indicates numerical instability. The results reported in Table 1 show that the symmetric formulation becomes unstable for sufficiently small values of γ , irrespectively of

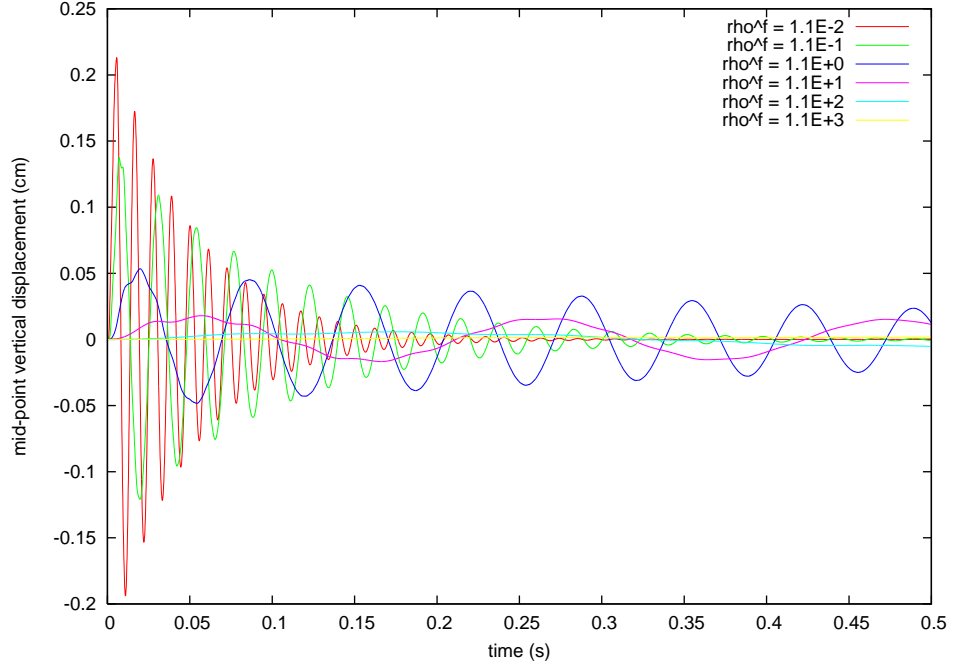


Figure 6: Stabilized explicit coupling ($K = 0$, $\alpha = 1$, $\gamma = 100$, $\gamma_0 = 8.75 \times 10^{-4}$): Interface mid-point y -displacement for different values of the fluid-solid density ratio ρ^f / ρ^s

$\gamma_0 \backslash \gamma$	1	10	100	1000	6000	10000	20000
1.75×10^{-5}	X	X	X	X	X	X	0.7739
3.5×10^{-5}	X	X	X	X	X	0.5183	0.7836
8.75×10^{-5}	X	X	X	X	X	0.5668	0.8115
1.75×10^{-4}	X	X	X	X	0.5216	0.6423	0.8534
3.5×10^{-4}	X	X	X	X	0.6792	0.7724	0.9209
8.75×10^{-4}	X	X	0.9104	0.9296	0.9793	1.0035	1.0169
1.75×10^{-3}	X	X	1.0676	1.0750	1.0615	1.0509	1.0331
3.5×10^{-3}	X	1.1568	1.1592	1.1737	1.1760	1.1762	1.1737
3.5×10^{-2}	X	1.7095	1.3270	1.3460	1.3474	1.3472	1.3466

Table 1: Stabilized explicit coupling ($K = 0$) with the symmetric formulation ($\alpha = 1$): out-flow relative errors

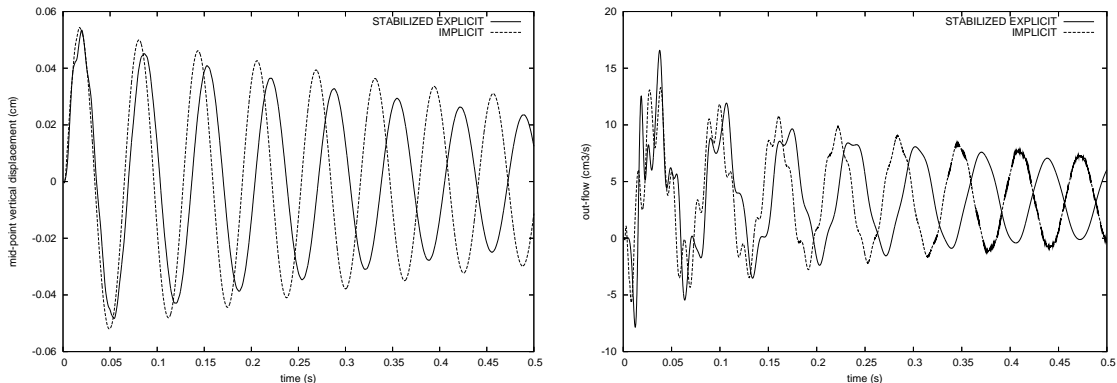


Figure 7: Interface mid-point y -displacement and out-flow: comparison of stabilized explicit coupling ($K = 0$, $\alpha = 1$, $\gamma = 100$, $\gamma_0 = 8.75 \times 10^{-4}$) and implicit coupling ($\alpha = 1$, $\gamma = 100$)

$\gamma_0 \backslash \gamma$	1	10	100	1000	6000	10000	20000
1.75×10^{-5}	X	X	X	X	X	X	0.7813
3.5×10^{-5}	X	X	X	X	X	0.5285	0.7910
8.75×10^{-5}	X	X	X	X	X	0.5772	0.8188
1.75×10^{-4}	X	X	X	X	0.5327	0.6528	0.8606
3.5×10^{-4}	X	X	X	X	0.6909	0.7831	0.9280
8.75×10^{-4}	X	X	0.9182	0.9425	0.9821	1.0140	1.0242
1.75×10^{-3}	X	X	1.0801	1.0870	1.0727	1.0617	1.0434
3.5×10^{-3}	1.2476	1.1578	1.1796	1.1918	1.1936	1.1936	1.1902
3.5×10^{-2}	1.5496	1.3987	1.3601	1.3566	1.3559	1.3556	1.3549

Table 2: Stabilized explicit coupling ($K = 0$) with the non-symmetric formulation ($\alpha = -1$): out-flow relative errors

γ_0 . In other words, we recover the stability condition $(31)_1$ for $\alpha = 1$. On the contrary, for the non-symmetric formulation, $\alpha = -1$, no positive lower bound is required on γ . As a result, the scheme remains stable, see Table 2, as long as we take a sufficiently large value of γ_0 according to the stability condition $(31)_3$. From Tables 1 and 2, we can also notice that larger values of γ allow stability with smaller values of γ_0 , which is still in agreement with the stability condition $(31)_3$. On the other hand, this numerical result illustrates that the accuracy of the scheme is the outcome of a balance between the two last terms appearing in the error estimate (44), namely,

$$\frac{C_{KT}^2 \gamma^2 \mu \delta t^2}{h^2} + \frac{\gamma_0 T}{\mu} \delta t.$$

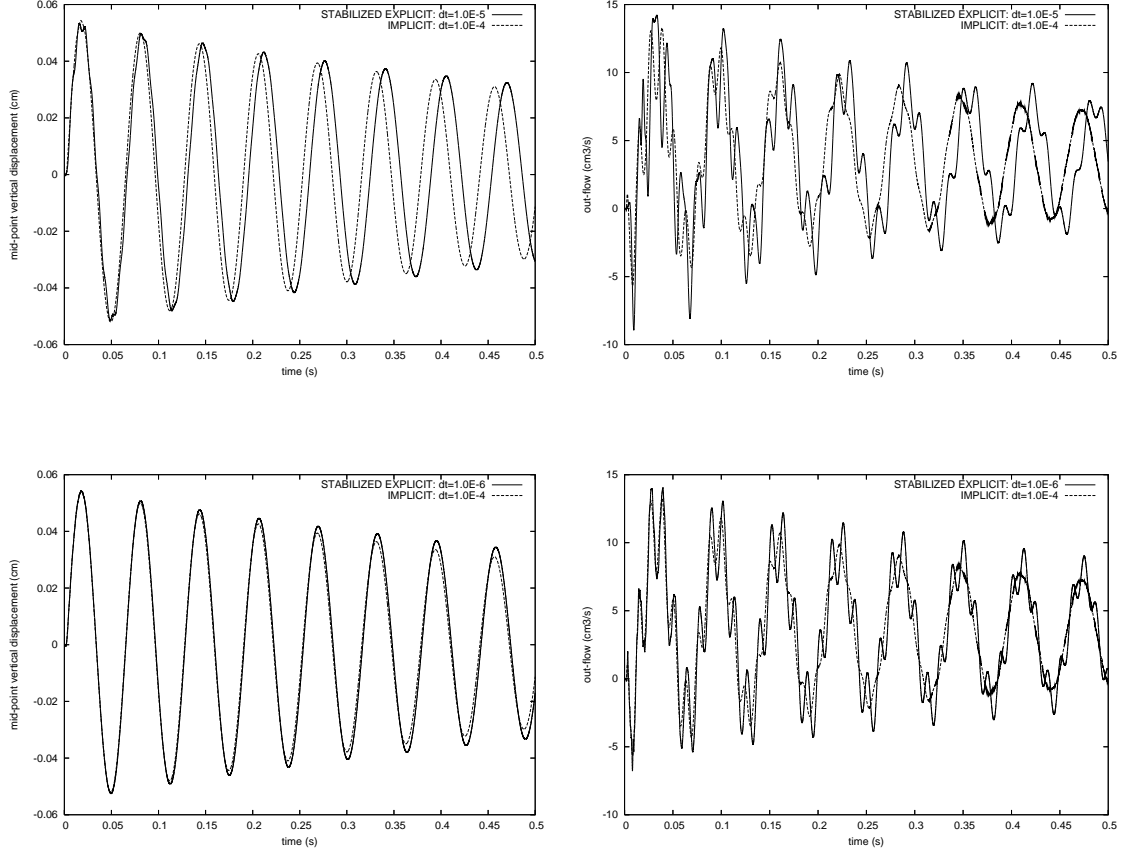


Figure 8: Interface mid-point y -displacement and out-flow, for $\delta t = 10^{-5}, 10^{-6}$, obtained with the stabilized explicit coupling ($K = 0$, $\alpha = 1$, $\gamma = 100$, $\gamma_0 = 8.75 \times 10^{-4}$) and with the implicit coupling ($\alpha = 1$, $\gamma = 100$), for $\delta t = 10^{-4}$

For large values of γ_0 the second term dominates, so that the accuracy is not much sensitive to changes in γ . For small values of γ_0 , on the other hand, the first term becomes prominent and the accuracy of the scheme more sensitive to γ . In particular, this shows that the procedure of improving the accuracy by increasing the Nitsche penalty γ and reducing the time penalty γ_0 , thanks to $(31)_3$, is limited by the impact of γ^2 on the error estimate (44).

Finally, in order to improve the accuracy of the solution, we consider the stabilized explicit coupling scheme (49)-(50) with one or two corrections ($K = 1, 2$). In Figures 9 and 10 we report a comparison with the implicit coupling scheme. After one correction step, the stabilized explicit coupling scheme achieves first order accuracy $O(\delta t)$. The enhanced accuracy is clearly visible (see Figure 5), in particular, in the outflow rate. After two correction steps it provides a solution almost undistinguishable from the implicit scheme solution. This is a clear

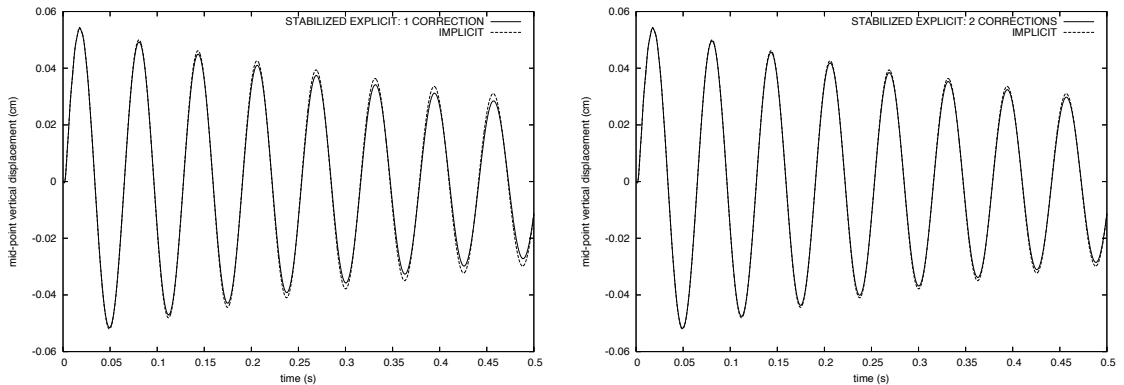


Figure 9: Interface mid-point y -displacement: stabilized explicit coupling with correction ($K = 1, 2$, $\alpha = 1$, $\gamma = 100$, $\gamma_0 = 3.5 \times 10^{-5}$) and implicit coupling ($\alpha = 1$, $\gamma = 100$)

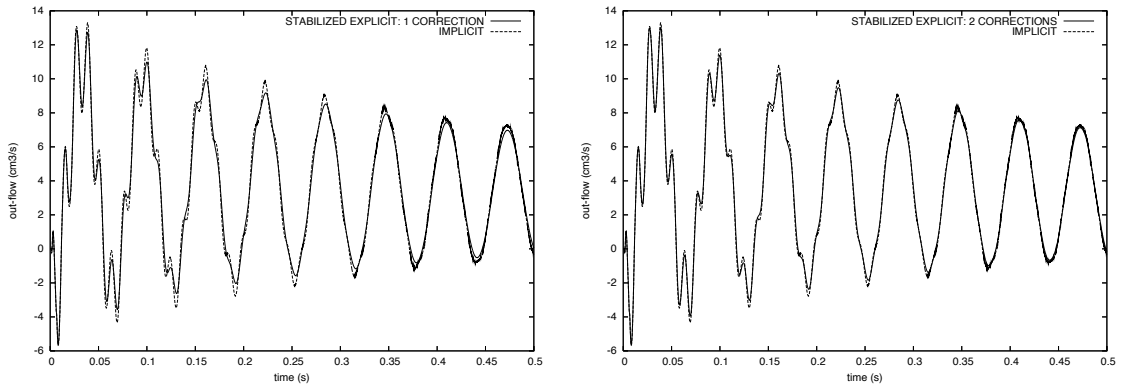


Figure 10: Out-flow: stabilized explicit coupling with correction ($K = 1, 2$, $\alpha = 1$, $\gamma = 100$, $\gamma_0 = 3.5 \times 10^{-5}$) and implicit coupling ($\alpha = 1$, $\gamma = 100$)

indication that, once the same order is reached (*i.e.* after one correction), further corrections are superfluous.

6.2 A three-dimensional test case

We now investigate the efficiency and accuracy of our stabilized explicit coupling scheme, with one correction ($K = 1$), by considering the 3D version of the numerical experiment analyzed in the previous paragraph.

The structure is described by the linear elasticity equations (Saint Venant-Kirchhof material), while the fluid is described by the incompressible Navier-

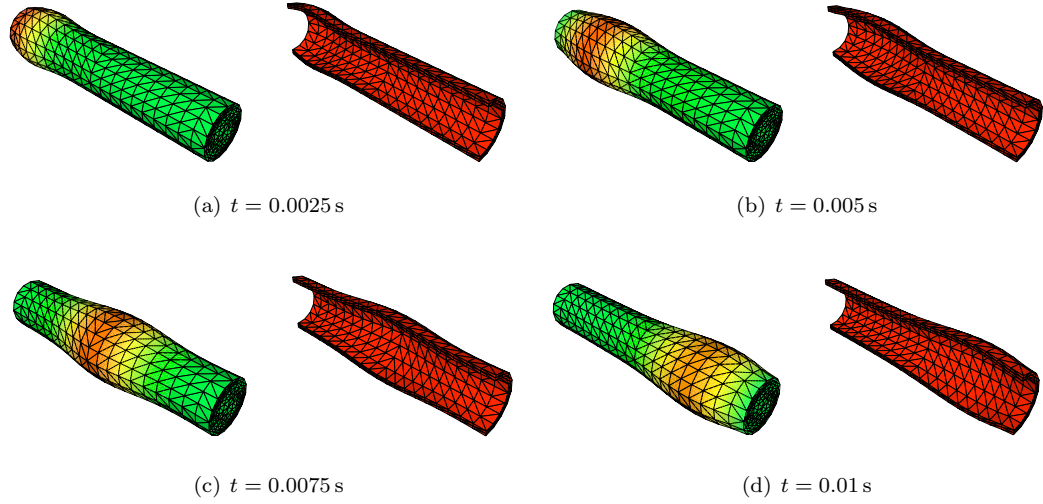


Figure 11: Straight vessel: snapshots of the pressure and solid deformation (exaggerated) at four time instants

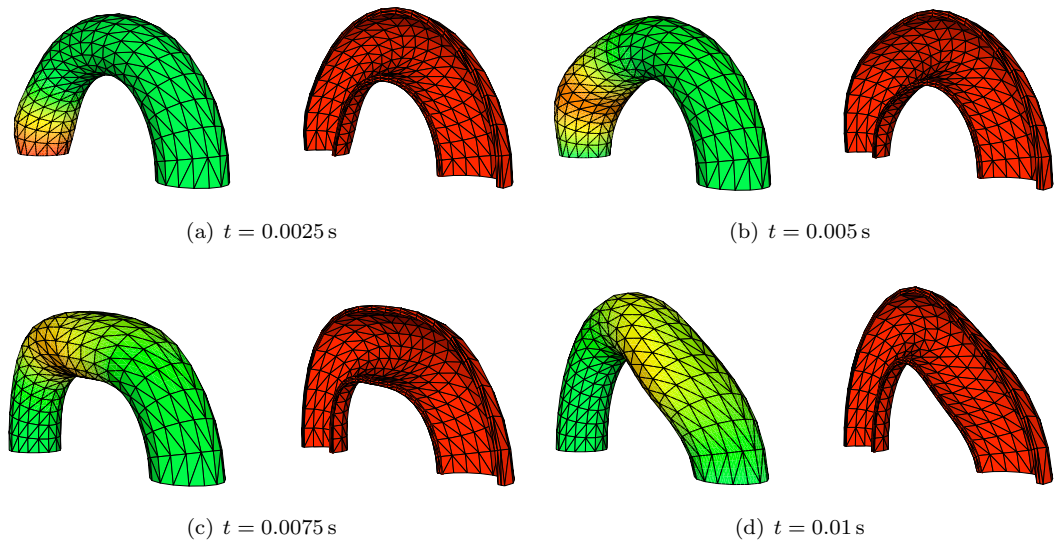


Figure 12: Curved vessel: snapshots of the pressure and solid deformation (exaggerated) at four time instants

Stokes equations with an ALE formulation (see *e.g.* [10]). As in [15], we consider two different geometries:

1. a straight vessel of radius 0.5 cm and length 5 cm,
2. a curved vessel of radius 0.5 cm with curvature ratio 0.25 cm^{-1} .

The surrounding structure has a thickness of 0.1 cm. The physical parameters are the following:

- Fluid: viscosity $\mu = 0.035$ poise, density $\rho^f = 1 \text{ g/cm}^3$,
- Solid: density $\rho^s = 1.2 \text{ g/cm}^3$, Young modulus $E = 3 \times 10^6 \text{ dynes/cm}^2$ and Poisson ratio $\nu = 0.3$.

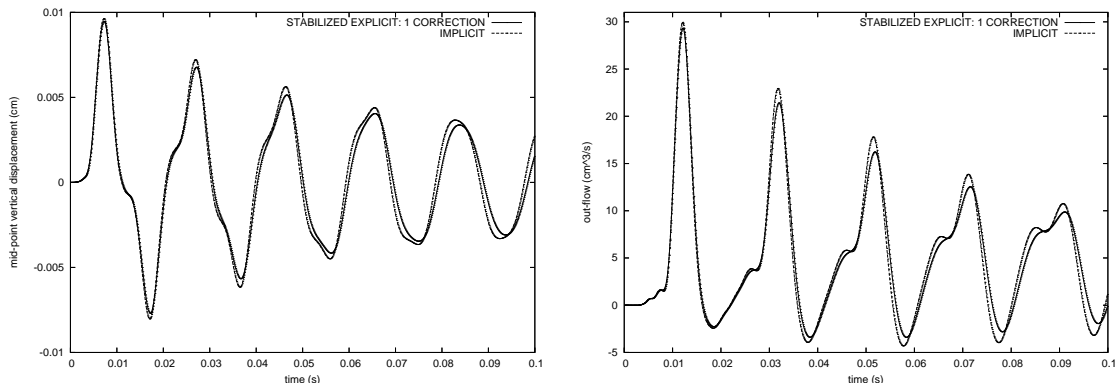


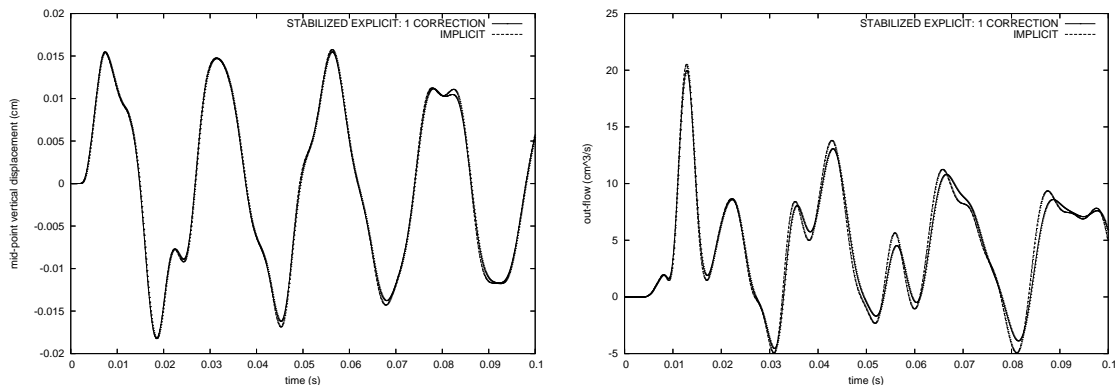
Figure 13: Straight vessel: interface mid-point y -displacement and out-flow

Both systems, the fluid and the structure, are initially at rest. The structure is clamped at the inlet and the outlet. An over pressure of $1.3332 \times 10^4 \text{ dynes/cm}^2$ is imposed, on the inlet boundary, during 5×10^{-3} seconds. The fluid equations are discretized using $\mathbb{P}_1/\mathbb{P}_1$ stabilized finite elements, whereas for the solid we use \mathbb{P}_1 finite elements. The time step is $\delta t = 10^{-4} \text{ s}$ and, for the Nitsche and time penalty parameters, we have taken $\gamma = 10$ and $\gamma_0 = 2.6 \times 10^{-5}$. The numerical computations have been performed within the framework of the LifeV finite element library (www.lifev.org).

A pressure wave propagation is observed in both configurations. Figures 11 and 12 show the fluid pressure and solid deformation (half a section) at the time instants $t = 0.0025, 0.005, 0.0075, 0.01 \text{ s}$. These results are in agreement with those provided in [15].

In Figures 13 and 14 we compare the interface mid-point y -displacement and out-flow rate obtained with the implicit coupling scheme, on one hand, and with stabilized explicit coupling scheme with one correction, on the other hand. As in the two-dimensional case, one correction is sufficient to recover the accuracy of the implicit coupling scheme.

Finally, in Table 3 we give the elapsed (dimensionless) CPU time for both schemes in the case of the curved vessel. We notice that the explicit coupling is 8 times faster than the implicit coupling, which is solved here using the partitioned Newton's method proposed in [15]. Obviously, this difference in performance is expected to increase when dealing, for instance, with non-linear solids and more complex geometries.

Figure 14: Curved vessel: interface mid-point y -displacement and out-flow

COUPLING	CPU time
Implicit	8
Stabilized explicit 1 correction	1

Table 3: Elapsed CPU time (dimensionless): 1000 time steps of length $\delta t = 10^{-4} s$.

7 Conclusion

In the present paper, we have proposed a stabilized explicit coupling scheme for the efficient solution of fluid-structure interaction problems involving a viscous incompressible fluid. The stability of the method is based on the Nitsche treatment of the interface coupling conditions, on one hand, and on the addition of a weakly consistent penalization of the (time) fluctuations of the fluid load at the interface, on the other hand. We show that the proposed explicit coupling scheme is stable irrespective of the fluid-solid density ratio.

The method is flexible with respect to the choice of time stepping schemes, for the fluid and the structure, and allows for independent meshing of both domains. The Nitsche based explicit coupling leads to a non-trivial interaction between the space and time parameters in the error analysis. In order to assure convergence (but not stability) the time-step has to be taken smaller than the space step, leading to a condition close to what is expected for the explicit time-stepping of parabolic problems. Stability, on the other hand, holds under a CFL-like condition, similar (in its structure, see Remark 5.4) to the one obtained for explicit schemes for hyperbolic problems.

In the present work we have deliberately considered only the simplest discrete formulation. The main ingredients for stability are

1. the dissipative properties of the Nitsche type coupling,
2. the physical dissipation in the fluid,

3. the addition of a stabilization term controlling the fluctuation of the fluid forces on the interface.

We have proposed to improve accuracy using a defect-correction approach. Numerical experiences have shown that one correction step allows to recover the accuracy of the underlying fully implicit scheme.

The present scheme provides a simple and robust approach to the explicit time stepping of fluid structure interaction problems involving a viscous incompressible fluid. The method, however, suffers from a deterioration of the accuracy. The success of the stabilized explicit coupling scheme depends on the possibility of finding an optimal set of parameters and a correction strategy that allows to improve the precision. We hope that the analysis and numerical experiments presented in this paper will stimulate further research in this direction.

References

- [1] S. Badia, F. Nobile, and C. Vergara. Fluid-structure partitioned procedures based on Robin transmission conditions. Technical Report 11, MOX, Politecnico di Milano, 2007.
- [2] K.J. Bathe and H. Zhang. Finite element developments for general fluid flows with structural interactions. *Int. J. Num. Meth. Engng.*, 2004.
- [3] R. Becker, P. Hansbo, and R. Stenberg. A finite element method for domain decomposition with non-matching grids. *M2AN Math. Model. Numer. Anal.*, 37(2):209–225, 2003.
- [4] E. Burman and M.A. Fernández. Stabilized explicit coupling for fluid-structure interaction using Nitsche’s method. *C. R. Math. Acad. Sci. Paris*, 345(8):467–472, 2007.
- [5] E. Burman and P. Hansbo. A unified stabilized method for Stokes’ and Darcy’s equations. *J. Comput. Appl. Math.*, 198:35–51, 2007.
- [6] E. Burman and P. Zunino. A domain decomposition method based on interior penalties for advection–diffusion–reaction problems. *Siam Jour. Num. Anal.*, 44:1612–1638, 2006.
- [7] P. Causin, J.-F. Gerbeau, and F. Nobile. Added-mass effect in the design of partitioned algorithms for fluid-structure problems. *Comput. Methods Appl. Mech. Engrg.*, 194(42–44):4506–4527, 2005.
- [8] S. Deparis, M. Discacciati, G. Fourestey, and A. Quarteroni. Fluid-structure algorithms based on Steklov-Poincaré operators. *Comput. Methods Appl. Mech. Engrg.*, 195(41–43):5797–5812, 2006.
- [9] S. Deparis, M.A. Fernández, and L. Formaggia. Acceleration of a fixed point algorithm for fluid-structure interaction using transpiration conditions. *M2AN Math. Model. Numer. Anal.*, 37(4):601–616, 2003.
- [10] J. Donéa, S. Giuliani, and J. P. Halleux. An arbitrary Lagrangian-Eulerian finite element method for transient dynamic fluid-structure interactions. *Comp. Meth. Appl. Mech. Engrg.*, pages 689–723, 1982.

-
- [11] C. Farhat and T. Lieu. A discussion of recent trends and claims pertaining to the staggered solution of FSI problems. In *Ninth U.S. National Congress on Computational Mechanics: USNCCM9*, San Francisco, July 23–26 2007.
- [12] C. Farhat, K. van der Zee, and Ph. Geuzaine. Provably second-order time-accurate loosely-coupled solution algorithms for transient nonlinear aeroelasticity. *Comput. Methods Appl. Mech. Engrg.*, 195(17–18):1973–2001, 2006.
- [13] M.A. Fernández, J.F. Gerbeau, and C. Grandmont. A projection semi-implicit scheme for the coupling of an elastic structure with an incompressible fluid. *Int. J. Num. Meth. Engrg.*, 69(4):794–821, 2007.
- [14] M.A. Fernández and M. Moubachir. An exact block-Newton algorithm for solving fluid-structure interaction problems. *C. R. Math. Acad. Sci. Paris*, 336(8):681–686, 2003.
- [15] M.A. Fernández and M. Moubachir. A Newton method using exact Jacobians for solving fluid-structure coupling. *Comp. & Struct.*, 83:127–142, 2005.
- [16] L. Formaggia, J.-F. Gerbeau, F. Nobile, and A. Quarteroni. On the coupling of 3D and 1D Navier-Stokes equations for flow problems in compliant vessels. *Comp. Meth. Appl. Mech. Engrg.*, 191(6-7):561–582, 2001.
- [17] C. Förster, W.A. Wall, and E. Ramm. Artificial added mass instabilities in sequential staggered coupling of nonlinear structures and incompressible viscous flows. *Comput. Methods Appl. Mech. Engrg.*, 196(7):1278–1293, 2007.
- [18] J.-F. Gerbeau and M. Vidrascu. A quasi-Newton algorithm based on a reduced model for fluid-structure interactions problems in blood flows. *Math. Model. Num. Anal.*, 37(4):631–648, 2003.
- [19] P. Hansbo. Nitsche’s method for interface problems in computational mechanics. *GAMM-Mitt.*, 28(2):183–206, 2005.
- [20] P. Hansbo and J. Hermansson. Nitsche’s method for coupling non-matching meshes in fluid-structure vibration problems. *Computational Mechanics*, 32(1–2):134–139, 2003.
- [21] P. Hansbo, J. Hermansson, and T. Svedberg. Nitsche’s method combined with space-time finite elements for ALE fluid-structure interaction problems. *Comput. Methods Appl. Mech. Engrg.*, 193:4195–4206, 2004.
- [22] F. Hecht, O. Pironneau, A. Le Hyaric, and K. Ohtsuka. *FreeFem++ v. 2.11. User’s Manual*. University of Paris 6.
- [23] E. Järvinen, P. Råback, and M. Lyly. Optimization of fluid-structure interaction scheme for arterial flow simulations. In *2nd International Symposium on Modelling of Physiological Flows – MPF 2005, Sesimbra, Portugal*, 2005.
- [24] W. Layton, H. K. Lee, and J. Peterson. A defect-correction method for the incompressible Navier-Stokes equations. *Appl. Math. Comput.*, 129(1):1–19, 2002.

- [25] P. Le Tallec and J. Mouro. Fluid structure interaction with large structural displacements. *Comput. Meth. Appl. Mech. Engrg.*, 190:3039–3067, 2001.
- [26] D. P. Mok and W. A. Wall. Partitioned analysis schemes for the transient interaction of incompressible flows and nonlinear flexible structures. In K. Schweizerhof W.A. Wall, K.U. Bletzinger, editor, *Trends in computational structural mechanics*, Barcelona, 2001. CIMNE.
- [27] D. P. Mok, W. A. Wall, and E. Ramm. Partitioned analysis approach for the transient, coupled response of viscous fluids and flexible structures. In W. Wunderlich, editor, *Proceedings of the European Conference on Computational Mechanics*. ECCM’99, TU Munich, 1999.
- [28] D. P. Mok, W. A. Wall, and E. Ramm. Accelerated iterative substructuring schemes for instationary fluid-structure interaction. In K.J. Bathe, editor, *Computational Fluid and Solid Mechanics*, pages 1325–1328. Elsevier, 2001.
- [29] H. Morand and R. Ohayon. *Fluid-Structure Interaction: Applied Numerical Methods*. John Wiley & Sons, 1995.
- [30] J. Nitsche. über ein Variationsprinzip zur Lösung von Dirichlet-Problemen bei Verwendung von Teilräumen, die keinen Randbedingungen unterworfen sind. *Abh. Math. Sem. Univ. Hamburg*, 36:9–15, 1971.
- [31] F. Nobile. *Numerical approximation of fluid-structure interaction problems with application to haemodynamics*. PhD thesis, EPFL, Switzerland, 2001.
- [32] K.C. Park, C.A. Felippa, and J.A. Deruntz. Stabilization of staggered solution procedures for fluid-structure interaction analysis. In Belytschko. T. and T.L. Geers, editors, *Computational Methods for Fluid-Structure Interaction Problems*, volume 26, pages 95–124. American Society of Mechanical Engineers, 1977.
- [33] S. Piperno. *Simulation numérique de phénomènes d’interaction fluide-structure*. PhD thesis, Ecole Nationale des Ponts et Chaussées, 1995.
- [34] S. Piperno. Explicit/implicit fluid/structure staggered procedures with a structural predictor and fluid subcycling for 2D inviscid aeroelastic simulations. *Internat. J. Numer. Methods Fluids*, 25(10):1207–1226, 1997.
- [35] A. Quaini and A. Quarteroni. A semi-implicit approach for fluid-structure interaction based on an algebraic fractional step method. *Math. Models Methods Appl. Sci.*, 17(6):957–983, 2007.
- [36] P. Råback, J. Ruokolainen, M. Lyly, and E. Järvinen. Fluid-structure interaction boundary conditions by artificial compressibility. In *ECCOMAS Computational Fluid Dynamics Conference, Swansea, UK*, 2001.
- [37] H.J. Stetter. The defect correction principle and discretization methods. *Numer. Math.*, 29:425–443, 1978.
- [38] T.E. Tezduyar. Finite element methods for fluid dynamics with moving boundaries and interfaces. *Arch. Comput. Methods Engrg.*, 8:83–130, 2001.

- [39] V. Thomée. *Galerkin finite element methods for parabolic problems*, volume 25 of *Springer Series in Computational Mathematics*. Springer-Verlag, Berlin, second edition, 2006.

Contents

1	Introduction	3
2	The coupled problem	4
3	Nitsche’s formulation: space semi-discretization	5
3.1	Stability	6
3.2	Partitioned formulation	7
4	Time discretization: coupling strategies	9
4.1	Implicit coupling	10
4.1.1	Stability analysis – implicit coupling	10
4.2	Explicit coupling	11
4.2.1	Stability analysis – explicit coupling	13
5	Stabilized explicit coupling	14
5.1	Stability analysis	16
5.2	Stabilization and artificial compressibility	18
5.3	Weak consistency and error estimates	19
5.4	Improving time accuracy: defect-correction iterations	22
6	Numerical experiments	24
6.1	A two-dimensional test case	24
6.2	A three-dimensional test case	30
7	Conclusion	33



Unité de recherche INRIA Rocquencourt
Domaine de Voluceau - Rocquencourt - BP 105 - 78153 Le Chesnay Cedex (France)

Unité de recherche INRIA Futurs : Parc Club Orsay Université - ZAC des Vignes
4, rue Jacques Monod - 91893 ORSAY Cedex (France)

Unité de recherche INRIA Lorraine : LORIA, Technopôle de Nancy-Brabois - Campus scientifique
615, rue du Jardin Botanique - BP 101 - 54602 Villers-lès-Nancy Cedex (France)

Unité de recherche INRIA Rennes : IRISA, Campus universitaire de Beaulieu - 35042 Rennes Cedex (France)

Unité de recherche INRIA Rhône-Alpes : 655, avenue de l'Europe - 38334 Montbonnot Saint-Ismier (France)

Unité de recherche INRIA Sophia Antipolis : 2004, route des Lucioles - BP 93 - 06902 Sophia Antipolis Cedex (France)

Éditeur
INRIA - Domaine de Voluceau - Rocquencourt, BP 105 - 78153 Le Chesnay Cedex (France)
<http://www.inria.fr>
ISSN 0249-6399